Annexin A1 drives macrophage skewing to accelerate muscle regeneration through AMPK activation

Simon McArthur[1,2,#], Gaëtan Juban[3,#], Thomas Gobbetti[2,#], Thibaut Desgeorges[3], Marine Theret[3], Julien Gondin[3], Juliana E Toller-Kawahisa[2,4], Christopher P Reutelingsperger[5], Bénédicte Chazaud[3], Mauro Perretti[2,6*] and Rémi Mounier[3*]

[1]Institute of Dentistry, Barts & the London School of Medicine & Dentistry, Queen Mary University of London, Newark Street, London E1 2AT, United Kingdom

[2]William Harvey Research Institute, Barts & the London School of Medicine & Dentistry, Queen Mary University of London, Charterhouse Square, London EC1M 6BQ, United Kingdom

[3]Université Claude Bernard Lyon 1, CNRS UMR-5310, INSERM U-1217, Institut NeuroMyoGène, Lyon, France

[4]Department of Biochemistry & Immunology, Ribeirao Preto Medical School, University of Sao Paulo, Avenida Banderiantes, 3900, Ribeirao Preto, Sao Paulo 14049-900, Brazil

[5]Department of Biochemistry, Maastricht University, Cardiovascular Research Institute Maastricht, Maastricht, The Netherlands

[6]Centre for Inflammation and Therapeutic Innovation, Queen Mary, University of London

[#]share first authorship

[*]share senior authorship

Correspondence: s.mcarthur@qmul.ac.uk, m.perretti@qmul.ac.uk and remi.mounier@univ-lyon1.fr

Summary

Understanding the circuits that promote an efficient resolution of inflammation is crucial to deciphering the molecular and cellular processes required to promote tissue repair. Macrophages play a central role in the regulation of inflammation, resolution and repair/regeneration. Using a model of skeletal muscle injury and repair, herein we identified Annexin A1 (AnxA1) as the extracellular trigger of macrophage skewing towards a pro-reparative phenotype. Brought into the injured tissue initially by migrated neutrophils, and then over-expressed in infiltrating macrophages, AnxA1 activated FPR2/ALX receptors and the downstream AMPK signalling cascade leading to macrophage skewing, dampening of inflammation and regeneration of muscle fibres. Mice lacking AnxA1 in all cells or in myeloid cells only displayed a defect in this reparative process. *In vitro* experiments recapitulated these properties, with AMPK null macrophages lacking AnxA1-mediated polarisation. Collectively, these data identified the AnxA1/FPR2/AMPK axis as an important pathway in skeletal muscle injury regeneration.

Keywords: macrophage switch, resolution of inflammation, tissue repair, skeletal muscle homeostasis

Introduction

An efficient inflammatory response is a necessary component of the reaction to injury or infection, but it is equally critical for this inflammatory response to be terminated in a timely and appropriate manner, enabling the restoration of tissue homeostasis (1, 2). Indeed, chronic inflammation that results from failure of resolution represents a major contributing factor to a multitude of pathologies, from arthritis to sepsis to dementia (3, 4)

An inflammatory reaction consists of the co-ordinated activity of numerous cells and soluble mediators, but a central role is played by the macrophage. These cells, whether resident in the tissue or recruited from circulating monocyte populations, are amongst the first responders to pathogen- or damage-associated molecular patterns, initiating endothelial activation and neutrophil recruitment (5). Beyond their roles as sentinels, macrophages are important drivers of the progression of an inflammatory response, acting to clear pathogens, effete cells and debris by phagocytosis (6), serving as antigen presenting cells to recruit the adaptive arm of the immune response (7), and ultimately enabling processes of tissue repair and resolution (8, 9). That one cell type is able to achieve this diverse array of functions is due in large part to its remarkable degree of phenotypic plasticity, and as such macrophages may exist in a wide variety of forms along a spectrum running from a largely pro-inflammatory state, often indicated as M1, to a primarily non-phlogistic and pro-resolving phenotype, termed M2 (10).

A number of factors promoting this phenotypic transformation have been studied including exposure to anti-inflammatory cytokines such as interleukin (IL)-10 and IL-4, and the phagocytic removal of cell debris, although a complete description of the underlying mechanisms is lacking (11). We and others have identified a key role for the intracellular signalling pathway governed by AMP-activated protein kinase (AMPK) (12–14). Activation of this pathway is required for efficient conversion of pro- to anti-inflammatory-type macrophages, and inhibition of such a response significantly attenuated recovery in a model of inflammatory skeletal muscle injury (13). Whilst AMPK is undoubtedly important in the phenotypic conversion of macrophages during the course of an inflammatory reaction, the nature of the extracellular trigger(s) for its stimulation remains unclear.

The protein annexin A1 (ANXA1) (15, 16) is a major driver of inflammatory resolution, promoting neutrophil apoptosis (17), non-phlogistic monocyte recruitment (18) and macrophage efferocytosis (19, 20). Moreover, we and others have recently provided evidence showing ANXA1 to promote an

anti-inflammatory macrophage phenotype in *in vitro* models of rheumatoid arthritis (21) and tumour growth (22), but how this translates to an *in vivo* situation is less clear. Against this background, we applied a well-characterised model of skeletal muscle injury (23–25) to test the hypothesis that ANXA1 and its receptor FPR2/ALX could be the upstream trigger of AMPK activation, and hence be a major driver of the pro- to anti-inflammatory macrophage phenotype shift, promoting inflammatory resolution and the restoration of skeletal muscle tissue homeostasis.

Results

Annexin A1 and Fpr2/3 null mice show impaired recovery from skeletal muscle injury

To investigate the role of ANXA1 and its receptor FPR2/ALX (in humans, or the orthologue Fpr2/3 in mice) in the control of macrophage phenotype we first utilised the murine model of cardiotoxin-induced *Tibialis Anterior* (TA) injury, a model characterised by necrotic tissue damage and extensive macrophage activity (13, 26).

Whilst uninjured TA muscle weight and myofibre size were comparable between wild-type, AnxA1$^{-/-}$ and Fpr2/3$^{-/-}$ mice (Fig 1A-B, Suppl Fig 1A-B), recovery of muscle mass following administration of cardiotoxin was significantly reduced in AnxA1$^{-/-}$ and Fpr2/3$^{-/-}$ mice than in wild-type animals (Fig 1B). Histological analysis of muscles 28 days post-injury revealed significantly reduced myofibre cross-sectional area (CSA) and myonuclei *per* fibre (*i.e.*, the result of differentiation and fusion of muscle stem cells) in AnxA1$^{-/-}$ and Fpr2/3$^{-/-}$ animals (Fig 1C-E). These outcomes are suggestive of impaired skeletal muscle regeneration, a notion confirmed by marked lipid accumulation in AnxA1$^{-/-}$ mice (Fig 1F, Suppl Fig 1D). Analysis of immune cell infiltration by flow cytometry revealed that 2 days following cardiotoxin administration, approximately 60% of macrophages expressed a pro-resolving, anti-inflammatory phenotype (CD45^{+}Ly6C/G^{neg}F4/80^{hi}) in wild-type mice, whilst AnxA1$^{-/-}$ and Fpr2/3$^{-/-}$ animals showed comparable levels of pro- (CD45^{+}Ly6C/G^{hi}F4/80^{low}) and anti-inflammatory (CD45^{+}Ly6C/G^{low}F4/80^{hi}) cells (Fig 1G, Suppl Fig 1E). Consequently, the resolution index (ratio of anti- to pro-inflammatory macrophages) of AnxA1$^{-/-}$ and Fpr2/3$^{-/-}$ mice was significantly lower than that of wild-type animals, indicative of a prolonged inflammatory response (Fig 1H). These results indicate that a proportion of pro-inflammatory macrophages failed to convert to an anti-inflammatory phenotype at the time of resolution in the absence of AnxA1 or Fpr2/3. Inactivation of the Fpr1 receptor, another member of the Fpr family, did not reproduce these results (Suppl Fig 1F-G), suggesting a specific role of the AnxA1-Fpr2/3 pathway in these settings of cardiotoxin induced muscle injury and repair.

Macrophages are the major source of AnxA1 in lesion recovery

The more pronounced effects of cardiotoxin in AnxA1$^{-/-}$ and Fpr2/3$^{-/-}$ mice indicate that this pathway exerts important regulatory functions in skeletal muscle injury. We then characterised AnxA1 and Fpr2/3 expression kinetics during skeletal muscle regeneration. Monitoring ANXA1 expression in the tissue revealed that while essentially non-detectable in uninjured tissue, the protein was transiently induced from day 1 to day 4 post-lesioning with much lower levels by day 7 (Fig 2A). AnxA1 mRNA

analysis on FACS-sorted cell populations (Fig 2B, Suppl Fig 3A) combined with immunostaining (Suppl Fig 3B-D) indicated that this mediator was primarily restricted to immune cells until day 2 post-lesioning. Whilst F4/80^{+} murine macrophages expressed AnxA1 at all time-points examined (Suppl Fig 3B-C), the proportion of macrophages expressing its primary receptor, Fpr2/3, decreased over time, from approximately 95% at day 2 to 70% at day 7 and finally to 5% two weeks post-lesioning, even though significant numbers of macrophages were still detected in the tissue (Suppl Fig 4B-C). Importantly, expression of Fpr2/3 on muscle fibres was not apparent at any time-point examined, as it was restricted to neutrophils and pro-inflammatory macrophages (Suppl Fig 4).

We next sought to functionally validate the role of this immune cell-derived ANXA1 using chimeric mice bearing wild-type muscle but AnxA1$^{-/-}$ bone marrow-derived leukocytes. Therefore, CX3CR1-GFP mice, which harbour GFP-expressing monocytes/macrophages were irradiated and transplanted with wild-type or AnxA1$^{-/-}$ derived bone marrow cells, prior to injection of cardiotoxin in the TA muscle (Fig 2C). Analysis of bone marrow populations at the time of euthanasia showed that less than 1% of monocytes (CD115^{pos} cells) expressed GFP, suggesting >99% engraftment efficiency with either wild-type or AnxA1$^{-/-}$ bone marrow (Suppl Fig 5B-C). Weight recovery was similar after wild-type or AnxA1$^{-/-}$ transplant (Suppl Fig 5A), but histological analysis of TA muscles 28-days post-CTX injury revealed that animals receiving AnxA1$^{-/-}$ bone marrow cells displayed a significantly reduced myofibre CSA than animals receiving wild-type bone marrow cells (Fig 2D-E). Since more than 90% of the macrophages present in the injured muscles originated from the transplanted marrow (Suppl Fig 5D-E), these data indicate that the defective regeneration quantified in AnxA1$^{-/-}$ muscle is a consequence of an intrinsic defect in myeloid, rather than stromal, cells.

Exogenous ANXA1 can induce human macrophage phenotype conversion in vitro

As our murine analyses indicate a potential role for AnxA1 in the polarisation of macrophages from a pro-inflammatory to a pro-resolving/reparative phenotype, we investigated these effects *in vitro* using human PBMC-derived macrophages. An M1-like macrophage phenotype was induced by 24 h incubation with bacterial lipopolysaccharide (LPS) and γ-interferon (IFNγ), prior to addition of human recombinant ANXA1 (hrANXA1). Following hrANXA1 treatment, analysis of cell surface markers revealed a significant reduction in expression of the M1 marker protein major histocompatibility complex II (MHCII) (Fig 3A), accompanied by a significant increase in expression of the M2 marker protein CD206 (Fig 3B). These surface marker changes were mirrored by changes at the transcriptional level, with hrANXA1 treatment inducing a reduction in mRNA expression for the pro-inflammatory genes *Tnfa* and *Nos2* paired with increased message of *Il-10* (Fig 3C-E). No significant

changes in *Tgfb1* expression were quantified (Fig 3F). Together, these *in vitro* data support our *in vivo* findings, providing evidence that ANXA1 application favours a pro-resolving macrophage phenotype.

Intriguingly, we observed significant FPR2/ALX surface expression both in unstimulated human PBMC-derived macrophages and M1-phenotype cells, yet cell surface expression of the receptor was lost on cells stimulated towards an M2 phenotype with IL-4 (Suppl Fig 4). These data are in agreement with the *in vivo* observation that Fpr2/3$^{-/-}$ is absent from macrophages that have infiltrated the injured muscle at Day 7 and beyond, that is, when a reparative cell phenotype has been acquired (Suppl Fig 2B-C). The functional engagement of FPR2/ALX was then confirmed through the use of the selective antagonist WRW_4. The modulatory effects of hrANXA1 on pro-inflammatory PBMC-derived macrophages (*i.e.* reduced surface MHCII expression and augmented surface CD206 expression) were lost in the presence of WRW_4 (Fig. 3G-H).

Together these experiments represent a clear *in vitro* counterpart to the effects observed in the muscle injury model, showing the key role of ANXA1 acting through FPR2/ALX to drive a shift in macrophage phenotype towards a pro-resolving and reparative polarisation.

Exogenous ANXA1 treatment stimulates AMPK activation through FPR2/ALX

The enzyme 5'-adenosine monophosphate-activated protein kinase, AMPK, plays a critical role in macrophage phenotype skewing and is necessary for efficient regeneration after skeletal muscle damage (13). We queried whether this signalling pathway would underlie the effects of hrANXA1 upon human macrophage phenotype and indeed muscle repair *in vivo*.

Exposure of human PBMC-derived macrophages to hrANXA1 activated a number of components of the AMPK signalling pathway, promoting phosphorylation of Ca^{2+}/calmodulin-dependent protein kinase II, AMPKα itself and its downstream effector acetyl-CoA carboxylase (Fig 4A-B). Interestingly, phosphorylation of these proteins in macrophages only occurred to an appreciable degree following exposure to hrANXA1 for 30-60 min (Fig 4B-D), in contrast to early MAP kinase signalling previously reported in human monocytes (18). That activation of AMPKα depended upon binding of hrANXA1 to FPR2/ALX was confirmed through analysis of the effects of the antagonist WRW_4, which abrogated hrANXA1-evoked AMPKα phosphorylation in human macrophages (Fig 4E). The specificity of hrANXA1 action through its human receptor FPR2/ALX was also determined with Fpr2/3$^{-/-}$ cells lacking the orthologue of the human FPR2/ALX (27). Analyses of murine BMDM from wild-type and

Fpr2/3$^{-/-}$ animals confirmed the pivotal role of this receptor: whilst treatment with hrANXA1 induced phosphorylation of AMPKα in wild-type cells, this response was absent in macrophages from Fpr2/3$^{-/-}$ mice (Fig 4F).

AMPK activation is required for macrophage phenotype conversion induced by ANXA1

We investigated the relationship between FPR2/ALX-mediated AMPK activation and the shift in macrophage phenotype induced by hrANXA1 treatment through analyses in primary BMDM taken from wild-type mice and animals lacking the key catalytic α_1 subunit of AMPK (28). Whilst treatment of wild-type macrophages with hrANXA1 (10 nM, 6h) reduced the percentage of cells positive for the pro-inflammatory markers iNOS and CCL3, this response was notably absent in cells from AMPKα1$^{-/-}$ mice (Fig 5A). Correspondingly, hrANXA1 treatment augmented the proportion of wild type cells expressing the anti-inflammatory markers TGFβ1 (notably at variance from human macrophages), CD163 and CD206, but this did not occur in cells lacking AMPKα1 (Fig 5B). Together, these data indicate activation of AMPKα1 as a key step in the macrophage phenotype shift induced by ANXA1.

To confirm these findings in human cells, we employed an RNA interference approach, transfecting primary PBMC-derived macrophages with three distinct siRNA constructs targeting the AMPKα1 subunit (Fig 5C). Treatment of M1-like pro-inflammatory macrophages for 6 h with 10 nM ANXA1 reduced the expression of MHCII and augmented that of CD206 in mock transfected cells and in cells bearing a non-targeting siRNA construct; this effect was absent in cells transfected with any of three different siRNA constructs targeting human AMPKα1 (Fig 5D-E, Suppl Fig 7A).

Adult myogenesis is ANXA1-AMPK signalling dependent in vitro

Together, data from the experiments with human and mouse macrophages make a compelling case that macrophage phenotype shifting can be induced through an ANXA1/FPR2/AMPK cascade. To investigate whether this process underlies differences in recovery from cardiotoxin-induced muscle lesions seen between wild-type and AnxA1$^{-/-}$ and Fpr2/3$^{-/-}$ mice, we made use of an established model of *in vitro* muscle repair (13, 29).

We employed an *in vitro* model of adult myogenesis in which conditioned medium from primary BMDM was used to stimulate primary murine myoblasts for 72h, quantifying the proportion of multinucleated myotubes (Fig 5F). As such this *in vitro* setting recapitulates the processes of adult myogenesis (activation, differentiation, migration and fusion of muscle cells) that occur during skeletal muscle regeneration (13, 29). Conditioned medium from ANXA1-treated wild-type

macrophages augmented the myotube fusion index (Fig 5G-I). This response was not observed when myotubes were treated with conditioned medium from ANXA1-treated AMPKα1$^{-/-}$ macrophages (Fig 5G-I). Direct addition of ANXA1 (10 nM) to myoblast cultures did not regulate the extent of cell fusion (Suppl Fig 7B).

Discussion

The timely resolution of inflammation is a fundamental requirement for restoring homeostasis following infection or damage, with its failure being a significant contributory factor to numerous chronic inflammatory pathologies. Macrophages are key players in this process, given their ability to transition from generally pro-inflammatory to anti-inflammatory phenotypes (7). Substantial effort has gone into deciphering the complex signals underpinning macrophage plasticity, with numerous soluble mediators having been implicated (11), but the mechanistic link between these factors and changes in phenotype remains poorly understood especially when investigated in specific tissue-restricted settings. In the current study, we have employed a well-characterised model of muscle injury and recovery (13) to identify the ability of myeloid cell-derived ANXA1 to promote an anti-inflammatory macrophage phenotype, promoting resolution and tissue repair. Moreover, we show the actions of this protein to be mediated through the cell surface receptor FPR2/ALX and downstream activation of the intracellular signalling molecule AMPK, mechanistically linking external and intracellular pro-resolving signals governing macrophage phenotype.

These data reinforce the identification of the ANXA1-FPR2/ALX pair as a major endogenous driver of inflammatory resolution, and add to its known roles in regulating neutrophil apoptosis (17), efferocytosis (20, 30), and the recruitment of monocytes to inflammatory sites (18). Notably, despite muscle tissue itself beginning to express ANXA1 during tissue repair, as noted previously (31), experiments with chimeric mice confirmed that in our experimental settings the most important source of the protein to enable muscle repair remains the myeloid cells themselves. Moreover, while previous studies have highlighted a direct plasma membrane action for extracellular ANXA1 in myoblast fusion *in vitro* (32, 33) our experiments indicate that Fpr2/3, the receptor target for ANXA1, is not expressed by stromal and parenchymal cells *in vivo*. This suggests that, at least in the context of skeletal muscle regeneration post-cardiotoxin application, the action of ANXA1 is mainly mediated by myeloid cells, which in turn regulate myogenic cells. While our studies do not absolutely identify whether neutrophils or macrophages are the primary source of endogenous ANXA1 within the injured tissue, neutrophils contain substantial amounts of this mediator (34), which we have previously shown to be a major monocyte chemoattractant (18), suggesting that the protein - produced at an early stage by and released from infiltrating neutrophils (35) - may act to both recruit monocytes and promote a pro-resolving phenotype in the resulting macrophages. Irrespective of the cell which is the source of ANXA1, the dependency upon the presence of ANXA1-expressing leukocytes for efficient macrophage phenotypic conversion is another example of how

"the beginning programs the end" in resolution (36), emphasising the finely tuned nature of the acute inflammatory response and its ability to encode its own termination.

Besides highlighting the role of ANXA1 as a regulator of inflammatory resolution (37), these data add further weight to the importance of its receptor FPR2/ALX in this process, identifying it as a major determinant for induction of a pro-resolving macrophage phenotype through AMPK activation. Of note, macrophage FPR2/ALX expression declined during the course of the response to muscular injury; congruently, FPR2/ALX expression was significantly lower in M2-like macrophages when compared with M1-like phenotype cells *in vitro*. This modulation of receptor expression may reflect a mechanism whereby once the macrophage is polarised towards a reparative phenotype, the utility of the FPR2/ALX signalling is no longer necessary.

There is considerable redundancy in the mediators known to induce the conversion of macrophage phenotypes, a feature that is perhaps expected given the importance of this cellular process to promote restoration of homeostasis after infection or damage; these factors include immune complexes, apoptotic cells and specific cytokines (38). Notably however, a significant proportion of these macrophage-polarising mediators derive from the adaptive arm of the immune response, particularly from T_H2 lymphocytes (11). Herein, we identify signalling components derived from the innate side of the immune system to promote resolution. Moreover, these results support the concept of how it is crucial to decipher mediators and signal(s) operative in specific tissues and organs to control macrophage polarisation hence to regulate the whole process of resolution and repair.

Our data associate activation of FPR2/ALX and the major regulator of cellular metabolism, AMPK, showing the central involvement of FPR2/ALX-stimulated AMPK pathway in the induction of a pro-resolving macrophage phenotype. The precise mechanism linking AMPK activation with a change in phenotype is as yet unclear, but there is increasing evidence that changes in the metabolic status of immune cells can affect their inflammatory activity (39, 40). Pro-inflammatory dendritic cells and T lymphocytes are characterised by high levels of glycolysis, akin to the Warburg metabolic shift described in cancer (41), whereas immune cells with an anti-inflammatory or pro-resolving profile tend to exhibit greater mitochondrial respiration (13, 42, 43). The mechanistic details of how such changes in metabolic phenotype relate to immune function, and indeed whether these differences reflect or drive immunophenotype, are not fully elucidated (44), but it is notable that AMPK is a significant promoter of mitochondrial respiration and a regulator of glycolysis through modulation of

lactate dehydrogenase activity (45), driven by its ability to respond to energy debt and an increased AMP:ATP ratio (46). Activation of this pathway is ideally placed to induce the metabolic phenotype most closely associated with anti-inflammatory macrophage activation, but this hypothesis requires further investigation.

AMPK is involved in different cellular mechanisms that regulate skeletal muscle homeostasis (47). Our previous findings highlighted the importance of crosstalk between AMPK and the mTOR signalling pathway for the control of muscle cell size in the adaptive response of skeletal muscle (48–51). Moreover, we have recently shown that AMPKα1, activated following phagocytosis, is crucial for macrophage skewing from a pro- to an anti-inflammatory phenotype during resolution (13), demonstrating that the CAMKKII/AMPKα1 cascade within macrophages is required for proper and complete skeletal muscle regeneration. Anti-inflammatory macrophages promote myogenic differentiation and fusion (29, 52, 53), a finding of importance for skeletal muscle regeneration where a sequential presence of pro- then anti-inflammatory cells is necessary for an efficient regeneration process (23, 24). We could demonstrate that macrophages conditioned by ANXA1, but not the soluble mediator itself, promoted myogenic fusion.

In summary, we present a mechanism governing the conversion of pro-inflammatory macrophages to a pro-resolving phenotype, linking leukocyte-derived ANXA1, FPR2/ALX and intracellular AMPK activation. Altogether, these data identify the ANXA1-FPR2/ALX pathway as a pivotal regulator of inflammatory resolution with non-redundant downstream actions on tissue repair. As such, ANXA1 and FPR2/ALX represent suitable targets for therapeutic exploitation for the innovative treatment of pathologies characterised by chronic, non-resolving inflammation.

Acknowledgments

This work was supported by CNRS, French Society of Myology and Wellcome Trust Programme Grant 086867/Z/08/Z. GJ was supported by Fondation pour la Recherche Médicale (Equipe FRM DEQ20140329495).

Author Contributions

SM, TG, GJ, JG, MT & RM performed TA lesion and analysis; GJ & RM produced and analyzed chimeric mice; SM, TG and JETK performed analysis of human macrophages; GJ, JG, MT & RM performed analysis of AMPKα1 null mice; TD & RM performed murine macrophages and myoblast fusion analysis; CPR produced and provided human recombinant ANXA1; SM, GJ, BC, MP & RM conceived and designed the study; all authors contributed to the drafting of the paper.

Declaration of Interests

MP is on the Scientific Advisory Board of ResoTher Pharma AS, interested in the development of Annexin A1-derived peptides for cardiovascular settings.

Figure Legends

Figure 1. Non-redundant role of ANXA1 in cardiotoxin-induced muscle injury and repair.

(A) Experimental set-up. Acute injury was induced by cardiotoxin (CTX) injection in the *Tibialis Anterior* (TA) of Wild-Type, AnxA1$^{-/-}$ and Fpr2/3$^{-/-}$ mice. Muscles were analysed 0, 7 and 28 days after injury. (B) TA mass normalised to mouse body weight. (C) Hematoxylin-eosin (HE) staining of muscles 28 days after injury. White bar = 50 µm. (D-E) Myofibre cross-sectional area (D), number of nuclei *per* myofibre (E) and lipid accumulation (F) in muscles 28 days post-CTX injury. (G-H) Macrophage subtypes analysis 2 days post-CTX injury. Shown are the percentage of pro- and anti-inflammatory macrophages within the F4/80^{+} population (G) and the resolution index (H). Results are mean ± SEM of at least three animals. *p<0.05, **p<0.01 and ***p<0.001 *versus* Wild-Type.

Figure 2. Infiltrating myeloid cell-derived ANXA1 controls muscle repair.

(A) Western blot analysis of ANXA1 protein in total *Tibialis Anterior* muscle. Muscles were analysed 0, 1, 2, 4, 7 and 14 days after injury. Shown are representative blots (top panel) and quantification of ANXA1 to β-actin (bottom panel) and ratios. (B) RT-qPCR analysis of Anxa1 mRNA level in various cell populations FACS-sorted from *Tibialis Anterior* muscle. Muscles were analysed 0, 1, 2, 4, 7 and 14 days after injury. (C) Experimental set-up of Bone Marrow Transplantation (BMT). CX3CR1-GFP mice were irradiated and then transplanted with bone marrow cells isolated from Wild-Type or AnxA1$^{-/-}$ mice. Bone marrow engraftment was checked on a blood sample after around 5 weeks. Then animals were injured in their *Tibialis Anterior* by cardiotoxin (CTX) injection and muscles analysed 0 or 28 days later. Engraftment was confirmed on the bone marrow of each animal on the day of sacrifice. (D-E) HE staining (D) and myofibre cross-sectional area (E) of TA muscles 28 days post-CTX injury. White bar = 50 µm. Results are mean ± SEM of at least two (D14 in A) or three muscles. *p<0.05 *versus* Wild-Type.

Figure 3. Exogenous hrANXA1 controls human and mouse macrophage polarisation *in vitro*.

Human PBMC-derived macrophages were incubated for 24 hours with LPS+IFNγ to promote an M1-like phenotype, prior to addition of human recombinant ANXA1 (hrANXA1, 10nM) for further 6 hours. (A-B) Median Fluorescent Intensity (MFI) units measured by flow cytometry of MHCII pro-inflammatory (A) and CD206 anti-inflammatory (B) markers. Shown are MFI quantification (left panel) and representative FACS plots (right panel). (C-F) RT-qPCR analysis of Tnfa (C) and Nos-2 (D) pro-inflammatory genes, and Il-10 (E) and Tgfb1 (F) anti-inflammatory genes. (G-H) MFI units as measured by flow cytometry of MHCII pro-inflammatory (G) and CD206 anti-inflammatory (H) markers after treatment by hrANXA1 in the presence or absence of the FPR2/ALX antagonist WRW_4

(10 µM). Experiments were performed on PBMC from 6 (A-F) or 3 (G-H) independent donors. Each colour represents an independent PBMC donor. *p<0.05 *versus* Vehicle. $^{\#}$p<0.05 *versus* Control.

Figure 4. The ANXA1/FPR2/ALX pathway activates the AMPK signalling cascade in human and murine macrophages.

(A) Schematic representation of the ANXA1/FPR2/ALX signalling cascade. (B-D) Western blot analysis of pCaMK, pAMPKα1 and pACC in human PBMC-derived macrophages treated with hrANXA1. Shown are representative blots (B) and quantification of pAMPKα1 to AMPKα1 (C) and pACC to ACC (D) ratios. (E) Representative western blot (top panel) and quantification (bottom panel) of pAMPKα1 to AMPKα1 ratio in human PBMC-derived macrophages treated by hrANXA1 in the presence or absence of 10 µM WRW_4. (F) Representative western blot (top panel) and quantification (bottom panel) of pAMPKα1 to AMPKα1 ratio in Wild-Type or Fpr2/3$^{-/-}$ murine bone marrow derived macrophages treated with hrANXA1. Results are means ± SEM of at least two (D) or three (C, E and F) independent experiments. *p<0.05, **p<0.01 *versus* Vehicle.

Figure 5. Null or reduced AMPK expression affects ANXA1-mediated macrophage polarisation.

(A-B) Primary macrophages derived from Wild-Type or AMPKα1$^{-/-}$ mice were treated with 10nM hrANXA1 and the percentage of cells expressing the pro-inflammatory markers iNOS and CCL3 (A) and the anti-inflammatory markers TGFB1, CD163 and CD206 (B) was determined by immunofluorescence. (C-E) Human PBMC-derived macrophages were transfected by a non-targeting or three different AMPKα1-targeting siRNAs and treated with 10 nM hrANXA1 for 24 h. AMPKα1 protein level was determined by FACS (C) and the MFI units of the pro-inflammatory MHCII (D) and anti-inflammatory CD206 (E) markers were measured by flow cytometry. (F-I) Conditioned medium produced by murine macrophages was transferred onto murine primary myoblasts and their fusion was measured by immunofluorescence. (F) Experimental set-up. (G) Representative images of desmin (red) and Hoechst (blue) labelling of myoblast cultures. White bar = 50 µm. (H-I) Fusion index calculated after desmin labelling. Shown are the means +/- SEM of the independent experiments relative to the Wild-Type Control (H) and the raw results of each individual replicate (I). Results are mean ± SEM of at least three independent experiments. *p<0.05 versus Mock or Control. $^{\#\#}$p<0.01 versus Wild-Type.

Suppl Fig 1. Related to Figure 1.

(A) HE staining of non-injured Wild-Type and AnxA1$^{-/-}$ *Tibialis Anterior* (TA) muscles. White bar = 50 µm. (B) Myofibre cross-sectional area of non-injured Wild-Type and AnxA1$^{-/-}$ TA muscles. Shown is

the mean +/- SEM of 8 muscles. (C) Number of nuclei *per* myofibre in muscles 7 days post-CTX injury. (D) Representative images of Sudan black staining of TA muscles from Wild-Type, AnxA1$^{-/-}$ and Fpr2/3$^{-/-}$ mice 28 days post-cardiotoxin injury. (E) Representative FACS plots of F4/80 and Ly6C/G markers in TA of Wild-Type, AnxA1$^{-/-}$ and Fpr2/3$^{-/-}$ mice 2 days post-cardiotoxin injury. (F-G) Macrophage subtypes analysis in Wild-Type and Fpr1$^{-/-}$ muscles 2 days post-CTX injury. Shown are the percentage of pro- and anti-inflammatory macrophages within the F4/80^{+} population (F) and the resolution index (G). Results are mean ± SEM of at least three animals. *p<0.05 *versus* Wild-Type.

Suppl Fig 2. Related to Figure 2. Gating strategy to isolate cell populations from *Tibialis anterior* muscle.

TA muscles were digested with Collagenase B/Dispase and cells were separated by magnetic beads based on their CD45 expression level. (A) CD45^{pos} cells were blocked with anti-FcgRII/III and labelled with CD45, CD64 and Ly6C antibodies to isolate Neutrophils (Neut) and Ly6C^{pos} and Ly6C^{neg} macrophages (Mac). Shown are representative plots for day 4 post-CTX injury together with purity check for recovered populations (coloured boxes). Numbers represent sorting purity calculated as percentage of live cells. (B) CD45^{neg} cells were labelled with CD45, CD31, Sca-1, α7-integrin and CD34 antibodies to isolate endothelial cells (EC), FAPs (FAP) and satellite cells (SAT). Shown are representative plots at day 4 (A) and day 1 (B) post-CTX injury, together with purity check for recovered populations (coloured boxes). Numbers represent sorting purity calculated as percentage of live cells.

Suppl Fig 3. Related to Figure 2. Immune cell recruitment and pattern of AnxA1 expression in cardiotoxin-induced muscle injury and repair.

(A) Anxa1 mRNA level measured by RT-qPCR on sorted cell populations from *Tibialis Anterior* muscle after cardiotoxin injury. (B-D) Immunofluorescence analysis of ANXA1 protein in *Tibialis Anterior* muscle after cardiotoxin injury. Images show co-localisation of ANXA1 protein with Ly6G^{+} (B) and F4/80^{+} (C) cells. White bar = 50 µm. (D) Quantification of F4/80^{+} ANXA1^{+} cells in *Tibialis Anterior* (TA) muscle after cardiotoxin (CTX) injury.

Suppl Fig 4. Related to Figure 2. Immune cell recruitment and Fpr2/3 expression in cardiotoxin-induced muscle injury and repair.

(A) Fpr2/3 mRNA level measured by RT-qPCR on sorted cell populations from *Tibialis Anterior* muscle after cardiotoxin injury. (B-C) Quantification of F4/80^{+} ANXA1^{+} cells in *Tibialis Anterior* (TA) muscle after cardiotoxin (CTX) injury. Representative immunofluorescence analysis of Fpr2/3 protein in TA

muscle after cardiotoxin (CTX) injury (B) and quantification of the percentage of F4/80^{+} cells expressing Fpr2/3 (C). White bar = 50 µm. Results are means ± SEM of three animals. *p<0.05 and ***p<0.001 *versus* Day 0.

Suppl Fig 5. Related to Figure 2. BMT controls

(A) Body weight follow-up, represented as percentage of Day 0, of mice after irradiation and bone marrow transplantation. Results are means ± SEM of at least six animals. *p<0.05 *versus* Day 0. (B-C) Representative FACS plots (B) and quantification (C) of the GFP^{+} monocytes in the bone marrow of the sacrificed animals. (D-E) Representative FACS plots (D) and quantification (E) of the percentage of macrophages with host or donor origin based on their GFP expression. Shown are TA muscles between day 2 and day 8 post-CTX injury.

Suppl Fig 6. Related to Figure 3. FPR2/ALX expression varies following human macrophage polarisation.

Human primary macrophages were polarised into M1 or M2 macrophages with IFNg and IL-4, respectively (A-C) Flow cytometry analysis of FPR2/ALX expression. Shown are representative FACS plots (A), percentage of cells expressing FPR2/ALX (B) and FPR2/ALX MFI (C). (D) RT-qPCR analysis of FPR2/ALX mRNA level. Results are means +/- SEM of at least four independent experiments. *p < 0.05 *versus* M0 (non-activated).

Suppl Fig 7. Related to Figure 5.

(A) Human PBMC-derived macrophages were transfected by a non-targeting or three different AMPKα1-targeting siRNAs and treated with 10 nM hrANXA1 for 24 h. AMPKα1 protein level was determined by western blot. (B) Primary myoblasts were differentiated for 3 days in presence of 10 nM hrANXA1 or conditioned medium produced by murine macrophages treated by 10 nM hrANXA1. Each dot corresponds to an independent experiment.

Methods

Animals

All procedures were performed under the UK Animals (Scientific Procedures) Act, 1986 in the UK or in compliance with European legislation in France. Animal facilities are fully licensed by relevant national authorities and protocols have been validated by local ethical committees. Male C57Bl/6 mice, male *alx/fpr2/3*$^{GFP/GFP}$ mice (referred to as Fpr2/3$^{-/-}$) bearing a knocked-in green fluorescent protein (27) and male *anxA1*$^{-/-}$ mice (54), aged 10 weeks were used for *in vivo* experiments. Both transgenic strains were fully backcrossed onto a C57Bl/6 genetic background.

Production of Recombinant Human Annexin A1

Human recombinant annexin A1 (hrANXA1) was produced by a prokaryotic expression system and purified essentially as described previously (55). Briefly, cDNA for human ANXA1 was inserted into the expression vector pQE30Xa (Qiagen) and transfected into E.coli (#SG13009 pREP4, Novagen) which were then grown in Luria-Bertani broth medium supplemented with ampicillin (50 µg/ml, Roche), kanamycin (30 µg/ml, Thermofisher) and 0.5% glycerol. Protein overexpression was initiated by addition of 5mM isopropyl β-D-1-thiogalactopyranoside (Eurogentec) and proteins were purified by IMAC. Purity and homogeneity were assessed by SDS-PAGE, western blotting and MALDI-TOF/TOF analysis. Endotoxin was determined with the Endosafe-PTS (FDA-licensed LAL cartridge from Charles-River) according to the manufacturer's protocol. HrANXA1 contained < 0.2 unit endotoxin *per* mg hrANXA1 protein.

Skeletal Muscle Injury

Skeletal muscle injury was caused by intramuscular injection of cardiotoxin (Latoxan) in the *Tibialis Anterior* (TA) muscle of male animals, as described previously (13). TA muscles were injected with cardiotoxin (50 µl *per* TA, 12 µM); 1, 2, 7, 14 or 28 days post-lesioning animals were killed by exposure to CO_2. TA were isolated and snap-frozen in liquid nitrogen-cooled isopentane for storage and later analysis. Only muscles harbouring more than 90 % of myofibres with centrally located nuclei were considered for analysis.

Murine Bone Marrow-Derived Macrophages

Bone marrow-derived macrophages (BMDMs) were prepared from adult male wild-type sv129/C57Bl6 and *Prkaa1*$^{-/-}$ mice (referred to as AMPKα1$^{-/-}$ (28)) . Mice were killed by cervical dislocation under isofluorane anaesthesia, and marrow was flushed from tibiae and femurs. Cells were plated, washed and grown for 6-7 days in DMEM High Glucose High Pyruvate, 20% heat

inactivated fetal calf serum (ThermoFisher), 30% L929-cell conditioned medium, 1% Amphotericin B (2.5 µg/ml, ThermoFisher) and 100 µg/ml streptomycin (ThermoFisher). For phenotypic characterisation, BMDMs were treated for 6 hours in presence or absence of 10 nM hrANXA1 and fixed for 10 minutes in 4% formaldehyde, permeabilized for 10 minutes in PBS with 0.5 % Triton X-100 and blocked for 1 hour in PBS with 4 % BSA. They were then labeled overnight at 4°C with anti-NOS2 (#ab15323, Abcam), anti-CCL3 (#ab32609, Abcam), anti-TGFβ1 (#ab64715, Abcam), anti-CD163 (#sc-20066, Santa-Cruz) and anti-CD206 (#sc-58987, Santa-Cruz), followed by incubation for 1 hour at 37°C with FITC- or Cy3-conjugated secondary antibodies (Jackson Immunoresearch Inc). Cells were stained with Hoechst (Sigma) and mounted in Fluoromount (Interchim) and pictures were taken on an Axio Imager.Z1 (Zeiss) at 20X of magnification connected to a CoolSNAP MYO CCD Camera (Photometrics).

***In vitro* model of adult myogenesis**

Macrophages were obtained from bone marrow (BM) precursor cells extracted from four distinct mice that were cultured in DMEM containing 20% FBS and 30% conditioned medium of L929 cell line (enriched in CSF-1) for 7 days. Macrophages were activated with human recombinant annexin A1 for 3 days (10 nM) in DMEM containing 10% FBS. After the washing steps, serum-free DMEM was added for 24 hr to obtain macrophage-conditioned medium. Murine myogenic precursor cells (MPCs) were obtained from TA muscle isolated from four mice and cultured using standard conditions in DMEM/F12 medium (Gibco Life Technologies) containing 20% heat inactivated Foetal Bovine Serum (FBS) and 2% G/Ultroser (Pall Inc). MPCs were seeded at 30,000 cell/cm^2 on Matrigel (diluted 1:10) and incubated for 3 days with conditioned medium containing 2% heat inactivated horse serum. In the case of direct treatment of MPCs, cells were directly incubated with 10 nM of hrANXA1 for 3 days in presence of 2% heat inactivated horse serum. Cells were then incubated with an anti-desmin antibody (#ab32362, Abcam), followed by a Cy3-conjugated secondary antibody (Jackson Immunoresearch Inc) (13, 29). Cells were stained with Hoechst (Sigma) and mounted in Fluoromount (Interchim) and pictures were taken on Axio Observer.Z1 (Zeiss) at 20X of magnification connected to a CoolSNAP HQ2 CCD Camera (Photometrics

Bone Marrow Transplantation

Bone Marrow Transplantation was performed as previously described (13, 56). Total bone marrow cells were isolated by flushing the tibiae and femurs of 8- to 20-week-old donor mice (wild-type or $AnxA1^{-/-}$ males) with RPMI-1640 / 10% FBS. They were transplanted into 8- to 12-week-old recipient $CX3CR1\text{-}GFP^{+/-}$ males (monocytes/macrophages expressing GFP) previously lethally irradiated for 10

min with a dose of 0.85 Gy/min in an X-RAD 320 (Precision X-Ray). Total bone marrow cells were injected (10^7 cells diluted in 100 µL of RPMI-1640 / 50 % mouse serum) into the retro-orbital vein of recipient mice. After transplantation, mice were fed with ciprofloxacin (10 mg/kg/day) in the drinking water for 3-weeks. Engraftment efficiency was determined on peripheral blood 5 weeks after the transplantation and on bone marrow when mice were sacrificed by FACS analysis. Briefly, red cells were lysed with ACK buffer and leukocytes were incubated with FcR Blocking Reagent (Miltenyi Biotec) for 20 min at 4°C. Finally, cells were labeled with an APC-conjugated anti-CD115 antibody for 30 min at 4°C and analysed on a BD FACS Canto II (BD Biosciences). DAPI was used as viability marker. Engraftment was determined as the percentage of monocytes not expressing GFP.

Human Peripheral Blood-Derived Macrophages

Human cells were prepared according to an approved protocol (East London & the City Local Research Ethics Committee; no. 06/Q605/40; P/00/029). Peripheral blood was collected from 6 different healthy volunteers by intravenous withdrawal in 3.2% sodium citrate solution (1:10). Peripheral blood mononuclear cells were isolated by density centrifugation on a Histopaque-1077 gradient (Sigma) according to the manufacturer's instructions, and were plated in RPMI 1640 for 1 hour. Cells were washed three times with ice-cold PBS without Ca^{2+}/Mg^{2+} to remove lymphocytes, and adherent cells were incubated in RPMI 1640 containing 20% heat inactivated fetal calf serum for 14 days.

Histological and Immunohistochemical Analysis

For histological analysis, muscles were harvested, snap frozen in liquid nitrogen-chilled isopentane and kept at -80°C until use. Cryosections (10µm) were prepared for hematoxylin-eosin (HE) or Sudan Black staining. Stained sections were scanned using an Axio Scan.Z1 (Zeiss) with a 20x objective an a 3 CCD HV-F 2025 CL camera (Hitachi) and Sudan Black labelled areas were quantified with ImageJ software. Briefly, images were converted into 8-bit binary image using "Yen" threshold filter and black pixels were numerated and expressed as a percentage of the total pixels in the muscle section. Fluorescence immunohistochemical analysis was performed according to standard procedures. Briefly, transverse muscle cryosections (10 µm) were post-fixed by incubation for 15 minutes in 4% formaldehyde, blocked and immunostained using primary antibodies directed against Ly6G (1:100; #127602, Biolegend), F4/80 (1:200, #123102, Biolegend) ANXA1 (1:1,000; #71-3400, ThermoFisher) or Fpr2/3 (1:100, #sc-18191-R, SantaCruz). Secondary antibodies were Alexa Fluor 488- or 594-conjugated goat anti-rabbit or anti-rat IgG (1:300; Invitrogen). Sections were counterstained with DAPI, mounted and examined using a TCS SP5 confocal laser scanning microscope (Leica

Microsystems) fitted with 405 nm, 488 nm and 594 nm lasers, and attached to a Leica DMI6000CS inverted microscope fitted with a 40× objective lens (NA 0.75 mm; working distance, 0.66 mm). Images were captured with Leica LAS AF 2.6.1 software and analysed using ImageJ 1.51w software (National Institutes of Health).

***In vivo* Macrophage Phenotype Analysis**

Macrophage phenotype was analyzed as previously described (13). Briefly, $CD45^+$ cells were isolated from regenerating muscle TA using magnetic beads conjugated to anti-CD45 antibody (Milteny Biotec) and then incubated with Fc-block (Milteny Biotec) for 30 min at 4°C. Finally, $CD45^+$ cells were stained with antibody against Ly-6C/G (#17-5931-82, eBioscience) and against F4/80 (#12-4801-82, eBioscience). Percentages of Ly-6C/G^{hi}F4/80^{low} and Ly-6C/G^{neg}F4/80^{hi} cells were calculated among total F4/80^{pos} cells following analysis by flow cytometry with a FACSCalibur instrument (Becton Dickinson, UK) and FlowJo v.9.2 analysis software as described below.

AMPKα1 siRNA

Primary human PBMC-derived macrophages were transfected with one of three different commercial siRNA sequences designed to target AMPKα1 or an Allstars negative control siRNA sequence using Hiperfect transfection reagent according to the manufacturer's instructions (final concentration 2 nM; all Qiagen GmbH, Hilden, Germany), alongside mock transfected cells. After 48 hours, cells were analysed for phenotypic conversion following hrANXA1 treatment (6 hours, 10 nM). A proportion of cells were analysed for AMPKα1 expression by western blot as described below or by flow cytometry. Briefly, 48h after siRNA transfection cells were detached, fixed by incubation in 4% formaldehyde in PBS at 4°C for 10 min, and permeabilised by resuspension with vortexing in ice-cold methanol. Surface FcγR were blocked by incubation for 20 min at 4°C with IgG block (ThermoFisher Scientific, UK) then incubated for 30 min at 4°C with a rabbit polyclonal antibody raised against the human AMPKα1 subunit (1:1,000, #2795, Cell Signalling Technology), followed by an AF488-conjugated goat anti-rabbit polyclonal secondary antibody (1:500, #A-11008, ThermoFisher Scientific, UK) staining. Cells were analysed on a FACS Canto II flow cytometer (BD Biosciences, UK) and using FlowJo 8.8.2 analysis software. A total of 10,000 singlet events were analysed for each sample.

Human Macrophage Flow Cytometry Analysis

Primary human PBMC-derived macrophages were labelled with FITC-conjugated mouse monoclonal anti-MHCII (#11-9956-42, Thermofisher) and APC-conjugated mouse monoclonal anti-CD206 (#17-

2069-42, Thermofisher) or isotype controls (all Thermofisher) according to manufacturer's protocols. In all cases, 20,000 events were acquired using a FACSCalibur flow cytometer (Becton Dickinson), and analysed using FlowJo analysis software (Version 9.2, Treestar Inc). In some cases, macrophages were analysed for surface expression of FPR2/ALX; surface FcγR were blocked by incubation for 20 minutes at 4°C with IgG block (ThermoFisher Scientific, UK), followed by incubation for 30 minutes at 4°C with mouse monoclonal anti-FPR2/ALX (1μg/106 cells; GM1D6, Aldevron, Freiburg, Germany) then incubation for 30 minutes at 4°C with secondary antibody (AF488-conjugated goat anti-mouse 1:300; ThermoFisher Scientific, UK).

Western Blot Analysis

Mouse muscle tissue and human macrophage samples were homogenised in RIPA buffer containing phosphatase and protease inhibitor cocktail (ThermoFisher Scientific, UK). Samples boiled in 6× Laemmli buffer were subjected to standard SDS-PAGE (10%) and electrophoretically blotted onto Immobilon-P polyvinylidene difluoride membranes (Millipore, Watford, UK). Membranes were incubated with antibodies raised against human phospho-Ca^{2+}/calmodulin-dependent kinase (#12716, Cell Signalling Technology), phospho-AMPKα (#2531, Cell Signalling Technology), AMPKα1 (#2795, Cell Signalling Technology), phospho-acetyl-CoA carboxylase (#3661, Cell Signalling Technology), acetyl-CoA carboxylase (#3662, Cell Signalling Technology, all 1:1000), ANXA1 (1:1000, #71-3400, ThermoFisher Scientific, UK) or β-actin (1:10,000; #A5316, Sigma) in Tris-buffer saline solution containing 0.1 % Tween-20 and 5 % (w/v) non-fat dry milk overnight at 4 °C. Membranes were washed for 30 minutes with Tris-buffer saline solution containing 0.1 % Tween-20, with the solution being changed at 10 minute intervals; membranes were then incubated with secondary antibody (horseradish peroxidase–conjugated goat anti-mouse 1:5000; ThermoFisher), for 2 hours at room temperature. Proteins were then detected using the enhanced chemiluminescence detection kit and visualized on Hyperfilm (Amersham Biosciences). Films were digitised and analysed using ImageJ 1.51w software (National Institutes of Health).

Quantitative RT-PCR

Total RNA was prepared from primary human PBMC-derived macrophages using TRIzol reagent (Life Technologies Ltd), and then reverse transcribed with superscript III reverse transcriptase (Life Technologies Ltd) according to the manufacturer's protocols. Resultant cDNA was then analysed by real-time PCR in duplicate, using the Quantitect primer system (Primer sets: FPR2/ALX QT00204295, IL-10 QT00041685, NOS-2 QT00068740, TNF-α QT00029162 and TGFβ1 QT00000728; all Qiagen Ltd.) and Power SYBR Green PCR Master Mix (Applied Biosystems). Reactions were performed in 384 well-

format using the ABI Prism 7900HT Sequence Detection System. The PCR conditions consisted of 95 °C 15 min, [95 °C 15 s – 55 °C 30 s – 72 °C 30 s] × 40, with a dissociation step [95 °C 15 s/60 °C 15 s/95 °C 15 s] included after the PCR reaction to confirm the absence of non-specific products. Data was acquired and analyzed with SDS 2.3 (Applied Biosystems); fold change was calculated as $2^{-\Delta\Delta Ct}$.

For Anxa1 and Fpr2/3 RT-qPCR analysis, cell populations were FACS-sorted from mouse *Tibialis Anterior* muscles as previously described (57) using a FACS Aria II cell sorter (BD Biosciences). Total RNA was isolated using NucleoSpin RNA Plus XS kit (Macherey-Nagel) and retro-transcribed into cDNA using Superscript II Reverse Transcriptase. qPCR was performed in triplicates on a CFX Connect™ Real-Time PCR Detection System (Bio-Rad) using LightCycler® 480 SYBR Green I Master (Roche Diagnostics). Calculation of relative expression was determined by the Bio-Rad CFX Manager™ software and fold change was normalised as Normalised Relative Quantity (or ΔΔCq) for each series, as $NRQ = \frac{2\Delta^{CqT-CqCal}}{2\Delta^{CqR-CqCal}}$ where T is the target sample, Cal is the calibrator value (*i.e.* the mean of all sample Cqs of the series) and R is the housekeeping gene Cyclophilin A. Sequence of primers used were as follows: 5'-GCACTCCAGCTTTCTTTGCC-3' (Anxa1 fwd), 5'-AATTTCCGAACGGGAGACCA-3' (Anxa1 rev), 5'-ACACCACAGGAACCGAAGAG-3' (Fpr2/3 fwd), 5'-TGGAGACAACCACCATTGAGA-3' (Fpr2/3 rev), 5'- GTGACTTTACACGCCATAATG -3' (Cyclophilin A fwd) and 5'- ACAAGATGCCAGGACCTGTAT -3' (Cyclophilin A rev).

Statistical Analysis

All quantified *in vitro* data are derived from at least three independent donors, with experiments performed in triplicate, and are expressed as mean ± SEM. Murine *in vivo* experiments were performed with a group size of n=6, sufficient to identify a 20% effect size with a power of 0.8, and are expressed as mean ± SEM. All mice were randomly allocated to groups, and analysis was performed blinded to experimental condition. Data were analysed by one- or two-way ANOVA as appropriate, with *post hoc* comparison using Tukey's HSD test. For murine *in vitro* experiments, at least 3 independent experiments were performed and statistical significance was determined using Student's t test. In all cases, a $P<0.05$ was taken as indicating statistical significance.

References

1. Perretti M, Cooper D, Dalli J, Norling L V. Immune resolution mechanisms in inflammatory arthritis. *Nat. Rev. Rheumatol.* 2017;13(2):87–99.

2. Serhan CN. Pro-resolving lipid mediators are leads for resolution physiology. *Nature* 2014;510(7503):92–101.

3. Perretti M, Leroy X, Bland EJ, Montero-Melendez T. Resolution Pharmacology: Opportunities for Therapeutic Innovation in Inflammation. *Trends Pharmacol. Sci.* 2015;36(11):737–755.

4. Tabas I, Glass CK. Anti-inflammatory therapy in chronic disease: challenges and opportunities.. *Science* 2013;339(6116):166–72.

5. Davies LC, Taylor PR. Tissue-resident macrophages: then and now. *Immunology* 2015;144(4):541–8.

6. Mantovani A, Biswas SK, Galdiero MR, Sica A, Locati M. Macrophage plasticity and polarization in tissue repair and remodelling. *J. Pathol.* 2013;229(2):176–85.

7. Motwani MP, Gilroy DW. Macrophage development and polarization in chronic inflammation. *Semin. Immunol.* 2015;27(4):257–266.

8. Lucas T et al. Differential Roles of Macrophages in Diverse Phases of Skin Repair. *J. Immunol.* 2010;184(7):3964–3977.

9. Troidl C et al. Classically and alternatively activated macrophages contribute to tissue remodelling after myocardial infarction. *J. Cell. Mol. Med.* 2009;13(9b):3485–3496.

10. Murray PJ et al. Macrophage Activation and Polarization: Nomenclature and Experimental Guidelines. *Immunity* 2014;41(1):14–20.

11. Martinez FO, Gordon S. The M1 and M2 paradigm of macrophage activation: time for reassessment. *F1000Prime Rep.* 2014;6:13.

12. Chan KL et al. Palmitoleate Reverses High Fat-induced Proinflammatory Macrophage Polarization via AMP-activated Protein Kinase (AMPK). *J. Biol. Chem.* 2015;290(27):16979–16988.

13. Mounier R et al. AMPKα1 regulates macrophage skewing at the time of resolution of inflammation during skeletal muscle regeneration. *Cell Metab.* 2013;18(2):251–64.

14. Park SY et al. SIRT1/Adenosine Monophosphate-Activated Protein Kinase α Signaling Enhances Macrophage Polarization to an Anti-inflammatory Phenotype in Rheumatoid Arthritis. *Front. Immunol.* 2017;8:1135.

15. Lim LHK, Pervaiz S. Annexin 1: the new face of an old molecule. *FASEB J.* 2007;21(4):968–975.

16. Perretti M, D'Acquisto F. Annexin A1 and glucocorticoids as effectors of the resolution of inflammation.. *Nat. Rev. Immunol.* 2009;9(1):62–70.

17. Solito E et al. A novel calcium-dependent proapoptotic effect of annexin 1 on human neutrophils.

FASEB J. 2003;17(11):1544–6.

18. McArthur S et al. Definition of a Novel Pathway Centered on Lysophosphatidic Acid To Recruit Monocytes during the Resolution Phase of Tissue Inflammation. *J. Immunol.* 2015;195(15):1500733.

19. Dalli J et al. Annexin A1 regulates neutrophil clearance by macrophages in the mouse bone marrow. *FASEB J.* 2012;26(1):387–96.

20. Scannell M et al. Annexin-1 and peptide derivatives are released by apoptotic cells and stimulate phagocytosis of apoptotic neutrophils by macrophages. *J. Immunol.* 2007;178(7):4595–605.

21. Rhys HI et al. Neutrophil Microvesicles from Healthy Control and Rheumatoid Arthritis Patients Prevent the Inflammatory Activation of Macrophages. *EBioMedicine* 2018;29:60–69.

22. Moraes LA et al. Annexin-A1 enhances breast cancer growth and migration by promoting alternative macrophage polarization in the tumour microenvironment. *Sci. Rep.* 2017;7(1):17925.

23. Arnold L et al. Inflammatory monocytes recruited after skeletal muscle injury switch into antiinflammatory macrophages to support myogenesis. *J. Exp. Med.* 2007;204(5):1057–69.

24. Varga T et al. Tissue LyC6- macrophages are generated in the absence of circulating LyC6- monocytes and Nur77 in a model of muscle regeneration. *J. Immunol.* 2013;191(11):5695–701.

25. Varga T et al. Highly Dynamic Transcriptional Signature of Distinct Macrophage Subsets during Sterile Inflammation, Resolution, and Tissue Repair. *J. Immunol.* 2016;196(11):4771–82.

26. d'Albis A, Couteaux R, Janmot C, Roulet A, Mira JC. Regeneration after cardiotoxin injury of innervated and denervated slow and fast muscles of mammals. Myosin isoform analysis. *Eur. J. Biochem.* 1988;174(1):103–10.

27. Dufton N et al. Anti-inflammatory role of the murine formyl-peptide receptor 2: ligand-specific effects on leukocyte responses and experimental inflammation. *J. Immunol.* 2010;184(5):2611–9.

28. Jørgensen SB et al. Effects of α-AMPK knockout on exercise-induced gene activation in mouse skeletal muscle. *FASEB J.* 2005;19(9):1146–1148.

29. Varga T et al. Macrophage PPARγ, a Lipid Activated Transcription Factor Controls the Growth Factor GDF3 and Skeletal Muscle Regeneration. *Immunity* 2016;45(5):1038–1051.

30. Maderna P, Yona S, Perretti M, Godson C. Modulation of phagocytosis of apoptotic neutrophils by supernatant from dexamethasone-treated macrophages and annexin-derived peptide Ac(2-26). *J. Immunol.* 2005;174(6):3727–33.

31. Bizzarro V, Belvedere R, Dal Piaz F, Parente L, Petrella A. Annexin A1 induces skeletal muscle cell migration acting through formyl peptide receptors. *PLoS One* 2012;7(10):e48246.

32. Leikina E et al. Extracellular annexins and dynamin are important for sequential steps in myoblast fusion. *J. Cell Biol.* 2013;200(1):109–123.

33. Bizzarro V et al. Role of Annexin A1 in mouse myoblast cell differentiation. *J. Cell. Physiol.*

2010;224(3):757–765.

34. Francis JW, Balazovich KJ, Smolen JE, Margolis DI, Boxer LA. Human neutrophil annexin I promotes granule aggregation and modulates Ca(2+)-dependent membrane fusion. *J. Clin. Invest.* 1992;90(2):537–44.

35. Damazo AS, Yona S, Flower RJ, Perretti M, Oliani SM. Spatial and temporal profiles for anti-inflammatory gene expression in leukocytes during a resolving model of peritonitis. *J. Immunol.* 2006;176(7):4410–8.

36. Serhan CN, Savill J. Resolution of inflammation: the beginning programs the end. *Nat. Immunol.* 2005;6(12):1191–7.

37. Leoni G, Nusrat A. Annexin A1: shifting the balance towards resolution and repair. *Biol. Chem.* 2016;397(10):971–9.

38. Amici SA, Dong J, Guerau-de-Arellano M. Molecular Mechanisms Modulating the Phenotype of Macrophages and Microglia. *Front. Immunol.* 2017;8:1520.

39. O'Neill LAJ, Kishton RJ, Rathmell J. A guide to immunometabolism for immunologists. *Nat. Rev. Immunol.* 2016;16(9):553–565.

40. Pearce EL, Pearce EJ. Metabolic pathways in immune cell activation and quiescence. *Immunity* 2013;38(4):633–43.

41. Rodriguez-Prados J-C et al. Substrate Fate in Activated Macrophages: A Comparison between Innate, Classic, and Alternative Activation. *J. Immunol.* 2010;185(1):605–614.

42. Jha AK et al. Network Integration of Parallel Metabolic and Transcriptional Data Reveals Metabolic Modules that Regulate Macrophage Polarization. *Immunity* 2015;42(3):419–430.

43. Tannahill GM et al. Succinate is an inflammatory signal that induces IL-1β through HIF-1α. *Nature* 2013;496(7444):238–242.

44. Van den Bossche J, O'Neill LA, Menon D. Macrophage Immunometabolism: Where Are We (Going)? *Trends Immunol.* 2017;38(6):395–406.

45. Theret M et al. AMPKα1-LDH pathway regulates muscle stem cell self-renewal by controlling metabolic homeostasis. *EMBO J.* 2017;36(13):1946–1962.

46. Mounier R, Théret M, Lantier L, Foretz M, Viollet B. Expanding roles for AMPK in skeletal muscle plasticity. *Trends Endocrinol. Metab.* 2015;26(6):275–86.

47. Kjøbsted R et al. AMPK in skeletal muscle function and metabolism. *FASEB J.* 2018;32(4):1741–1777.

48. Lantier L et al. AMPK controls exercise endurance, mitochondrial oxidative capacity, and skeletal muscle integrity. *FASEB J.* 2014;28(7):3211–24.

49. Lantier L et al. Coordinated maintenance of muscle cell size control by AMP-activated protein

kinase. *FASEB J.* 2010;24(9):3555–61.

50. Mounier R et al. Antagonistic control of muscle cell size by AMPK and mTORC1. *Cell Cycle* 2011;10(16):2640–6.

51. Mounier R et al. Important role for AMPKalpha1 in limiting skeletal muscle cell hypertrophy. *FASEB J.* 2009;23(7):2264–73.

52. Saclier M et al. Differentially activated macrophages orchestrate myogenic precursor cell fate during human skeletal muscle regeneration. *Stem Cells* 2013;31(2):384–96.

53. Saclier M, Cuvellier S, Magnan M, Mounier R, Chazaud B. Monocyte/macrophage interactions with myogenic precursor cells during skeletal muscle regeneration. *FEBS J.* 2013;280(17):4118–30.

54. Hannon R et al. Aberrant inflammation and resistance to glucocorticoids in annexin 1-/- mouse. *FASEB J.* 2003;17(2):253–5.

55. Kusters DHM et al. Pharmacological Treatment with Annexin A1 Reduces Atherosclerotic Plaque Burden in LDLR-/- Mice on Western Type Diet.. *PLoS One* 2015;10(6):e0130484.

56. Perdiguero E et al. p38/MKP-1–regulated AKT coordinates macrophage transitions and resolution of inflammation during tissue repair. *J. Cell Biol.* 2011;195(2):307–322.

57. Juban G et al. AMPK Activation Regulates LTBP4-Dependent TGF-beta1 Secretion by Pro-inflammatory Macrophages and Controls Fibrosis in Duchenne Muscular Dystrophy. *Cell Rep.* 2018;25(8):2163-2176.e6.

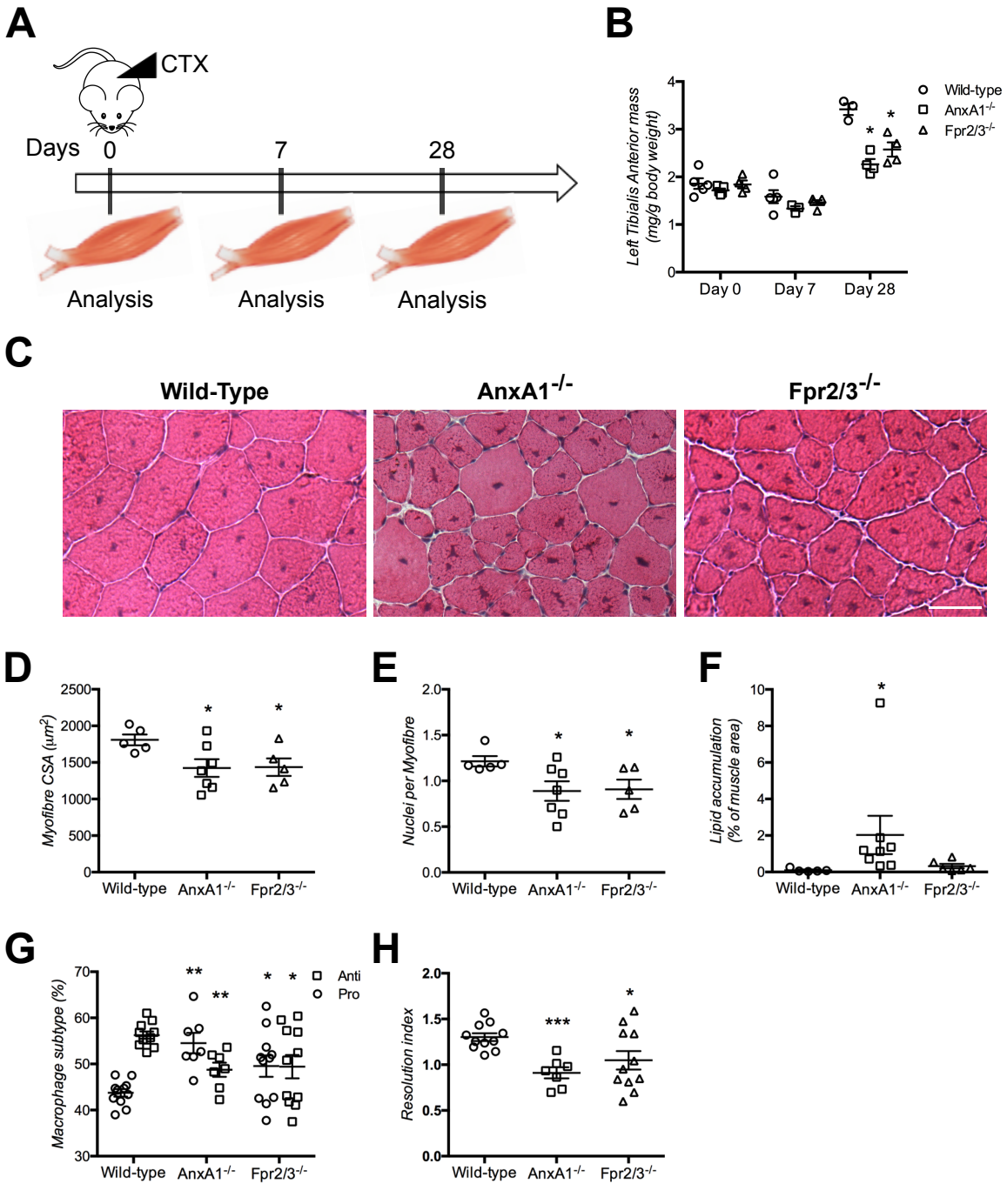
A
CTX
Days
0
7
28
Analysis
Analysis
Analysis
B
Left Tibialis Anterior mass (mg/g body weight)
Wild-type
AnxA1-/-
Fpr2/3-/-
Day 0
Day 7
Day 28
C
Wild-Type
AnxA1-/-
Fpr2/3-/-
D
Myofibre CSA (μm2)
E
Nuclei per Myofibre
F
Lipid accumulation (% of muscle area)
G
Macrophage subtype (%)
Anti
Pro
H
Resolution index
Wild-type
AnxA1-/-
Fpr2/3-/-

Figure 1

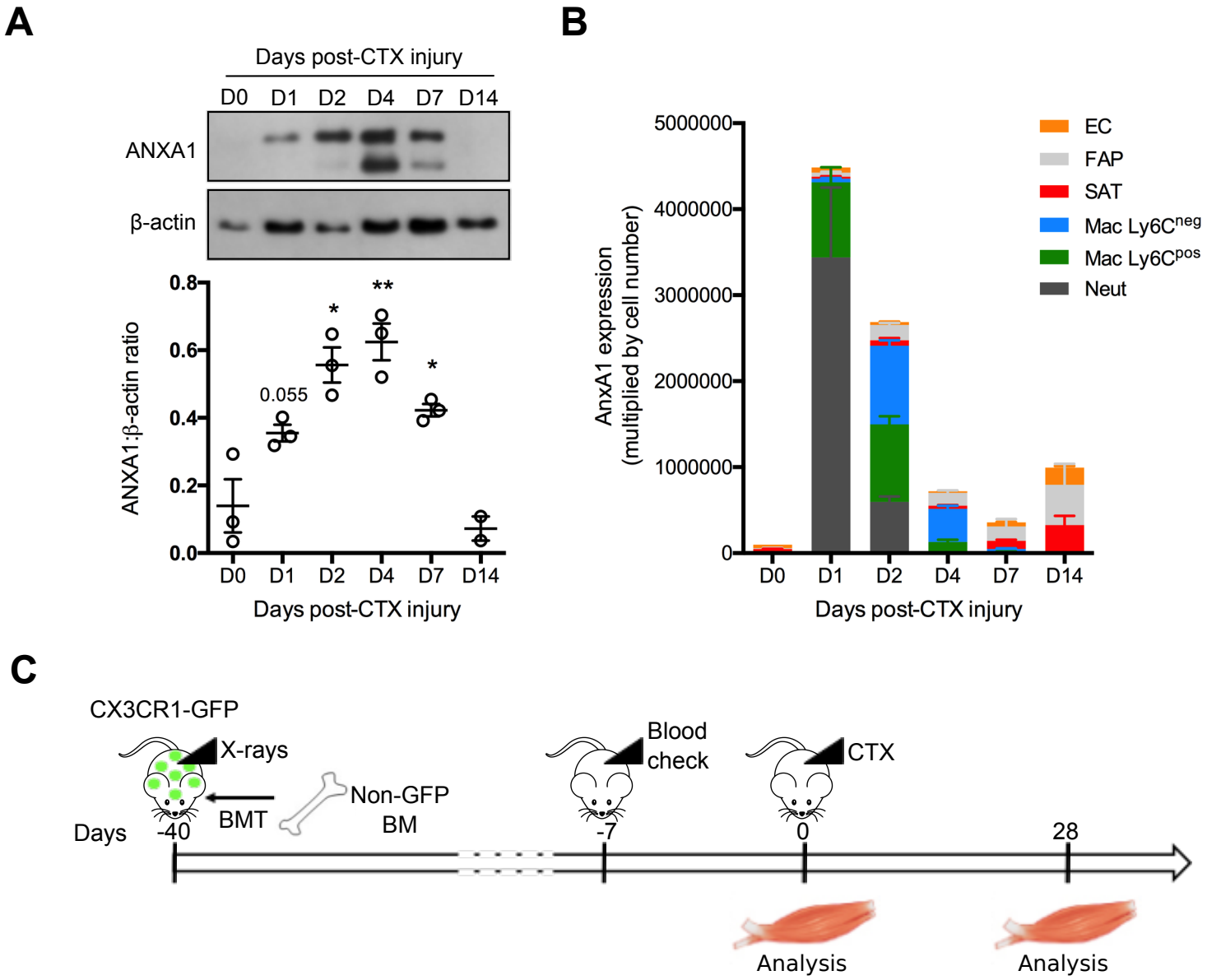
A
Days post-CTX injury
D0 D1 D2 D4 D7 D14
ANXA1
β-actin
ANXA1:β-actin ratio
0.055
Days post-CTX injury
B
AnxA1 expression (multiplied by cell number)
EC
FAP
SAT
Mac Ly6C^neg
Mac Ly6C^pos
Neut
Days post-CTX injury
C
CX3CR1-GFP
X-rays
BMT
Non-GFP BM
Blood check
CTX
Days
-40
-7
0
28
Analysis
Analysis
D
Wild-Type
AnxA1-/-
E
Myofibre CSA (µm²)
Wild-type
AnxA1-/-

Figure 2

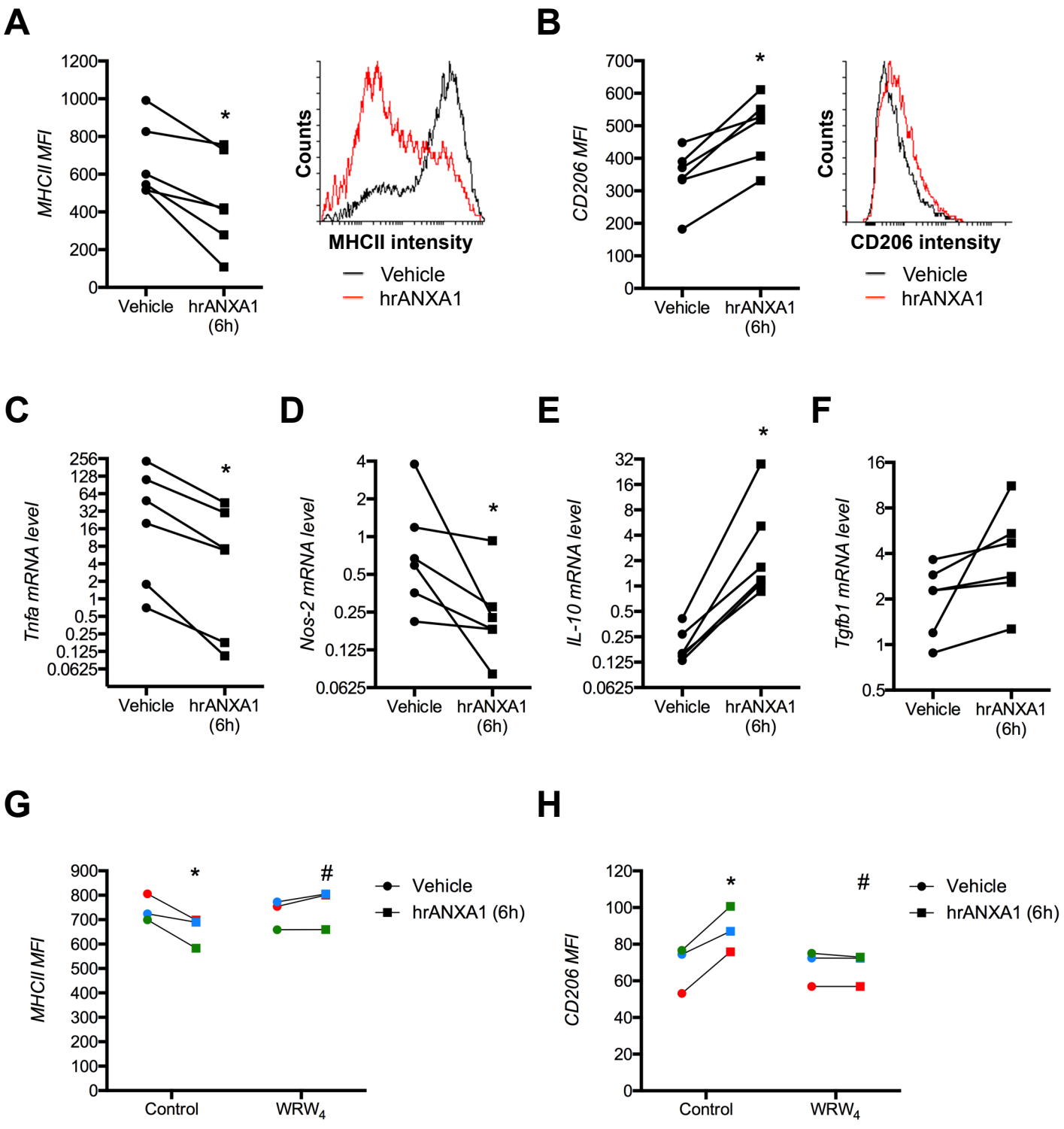
A
MHCII MFI
1200
1000
800
600
400
200
0
*
Vehicle
hrANXA1 (6h)
Counts
MHCII intensity
Vehicle
hrANXA1
B
CD206 MFI
700
600
500
400
300
200
100
0
*
Vehicle
hrANXA1 (6h)
Counts
CD206 intensity
Vehicle
hrANXA1
C
Tnfa mRNA level
256
128
64
32
16
8
4
2
1
0.5
0.25
0.125
0.0625
*
Vehicle
hrANXA1 (6h)
D
Nos-2 mRNA level
4
2
1
0.5
0.25
0.125
0.0625
*
Vehicle
hrANXA1 (6h)
E
IL-10 mRNA level
32
16
8
4
2
1
0.5
0.25
0.125
0.0625
*
Vehicle
hrANXA1 (6h)
F
Tgfb1 mRNA level
16
8
4
2
1
0.5
Vehicle
hrANXA1 (6h)
G
MHCII MFI
900
800
700
600
500
400
300
200
100
0
*
#
Control
WRW4
Vehicle
hrANXA1 (6h)
H
CD206 MFI
120
100
80
60
40
20
0
*
#
Control
WRW4
Vehicle
hrANXA1 (6h)

Figure 3

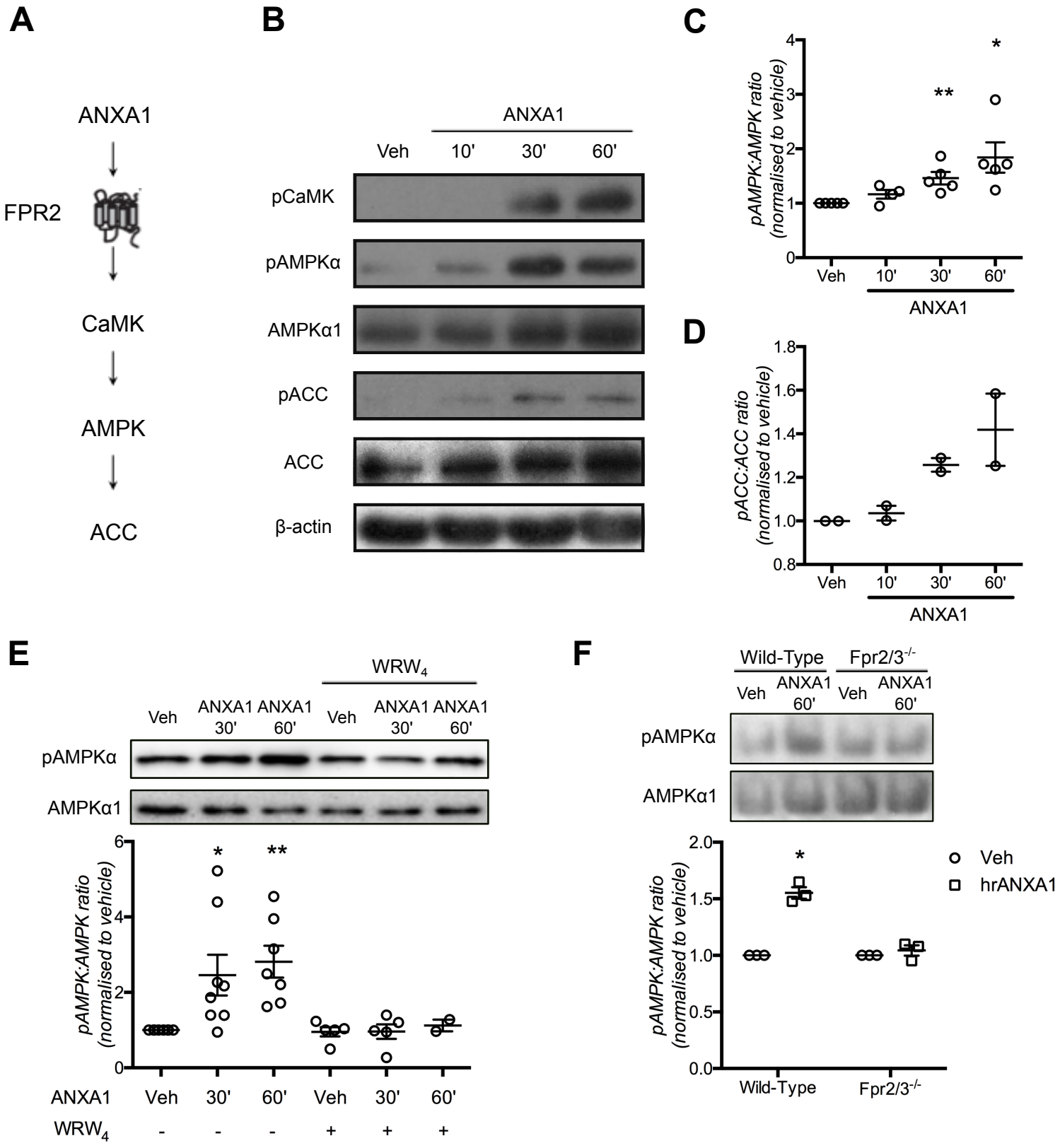
A
ANXA1
FPR2
CaMK
AMPK
ACC
B
ANXA1
Veh
10'
30'
60'
pCaMK
pAMPKα
AMPKα1
pACC
ACC
β-actin
C
pAMPK:AMPK ratio (normalised to vehicle)
Veh
10'
30'
60'
ANXA1
D
pACC:ACC ratio (normalised to vehicle)
Veh
10'
30'
60'
ANXA1
E
WRW4
Veh
ANXA1 30'
ANXA1 60'
pAMPKα
AMPKα1
pAMPK:AMPK ratio (normalised to vehicle)
ANXA1
WRW4
F
Wild-Type
Fpr2/3-/-
Veh
ANXA1 60'
pAMPKα
AMPKα1
pAMPK:AMPK ratio (normalised to vehicle)
Veh
hrANXA1
Wild-Type
Fpr2/3-/-

Figure 4

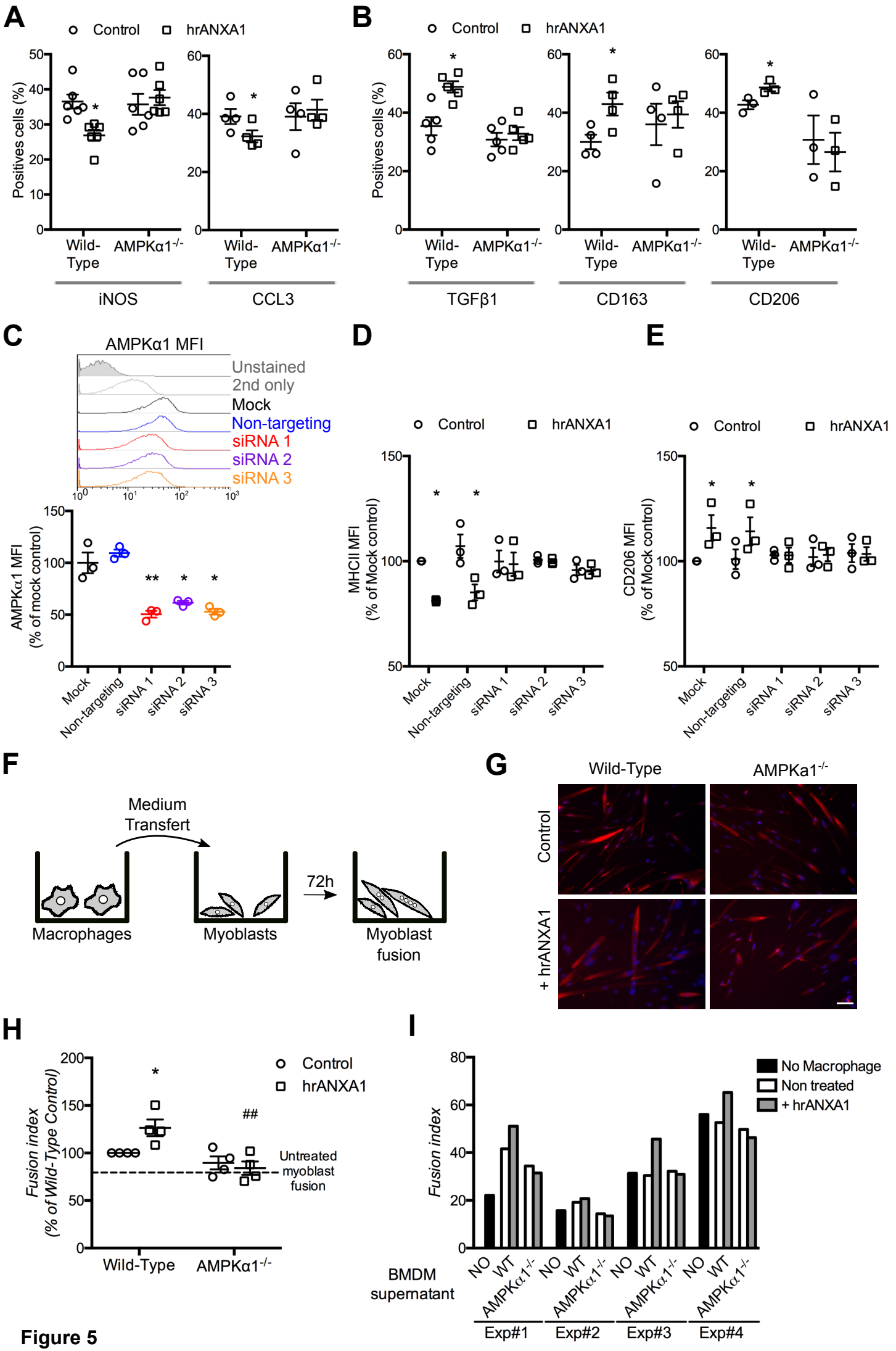
A
Control
hrANXA1
Positives cells (%)
Wild-Type
AMPKα1-/-
iNOS
CCL3
B
TGFβ1
CD163
CD206
C
AMPKα1 MFI
Unstained
2nd only
Mock
Non-targeting
siRNA 1
siRNA 2
siRNA 3
AMPKα1 MFI (% of mock control)
D
MHCII MFI (% of Mock control)
E
CD206 MFI (% of Mock control)
F
Medium Transfert
72h
Macrophages
Myoblasts
Myoblast fusion
G
Wild-Type
AMPKa1-/-
Control
+ hrANXA1
H
Fusion index (% of Wild-Type Control)
Untreated myoblast fusion
I
Fusion index
No Macrophage
Non treated
+ hrANXA1
BMDM supernatant
NO
WT
AMPKα1-/-
Exp#1
Exp#2
Exp#3
Exp#4

Figure 5

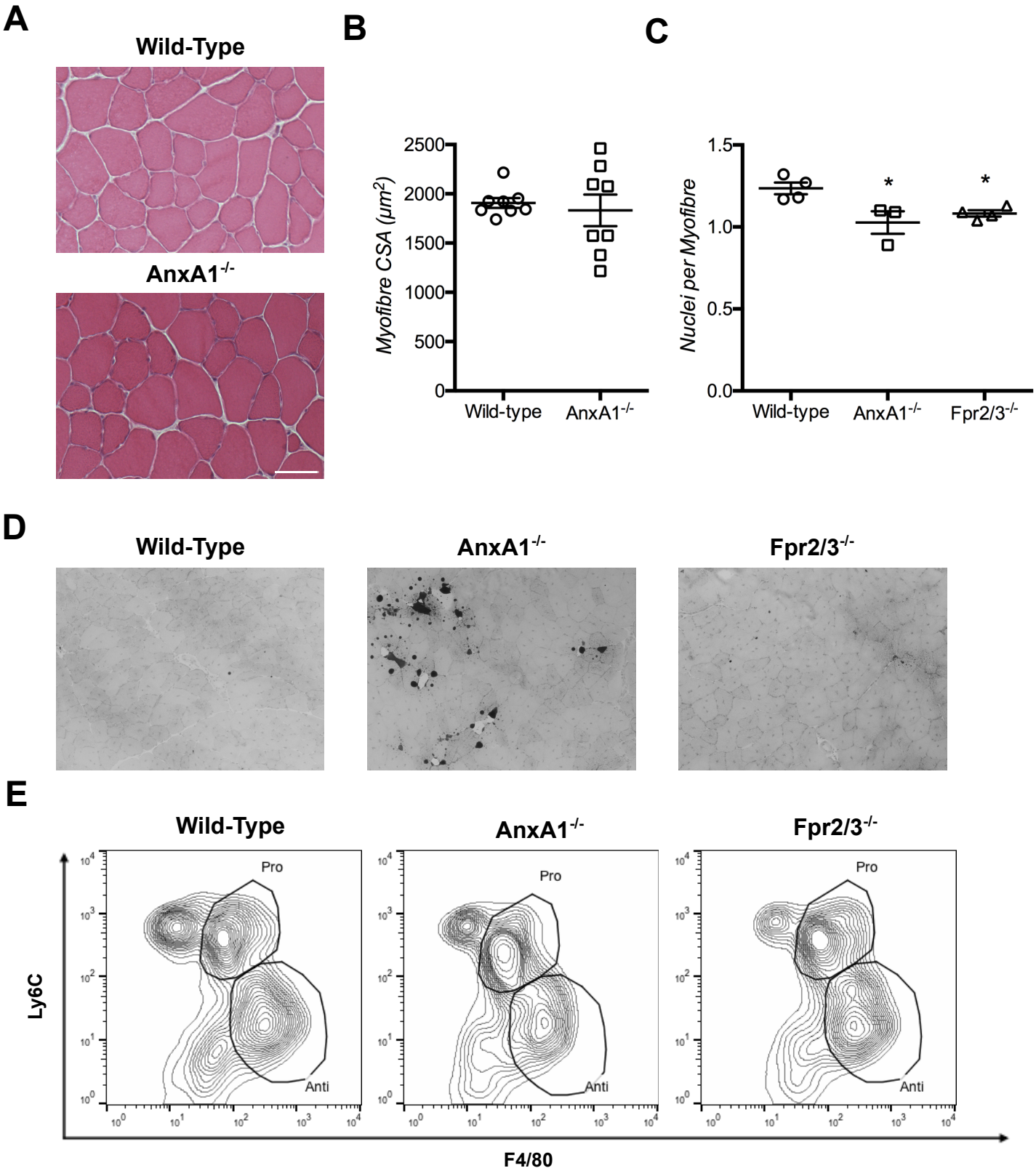

Supplementary Figure 1

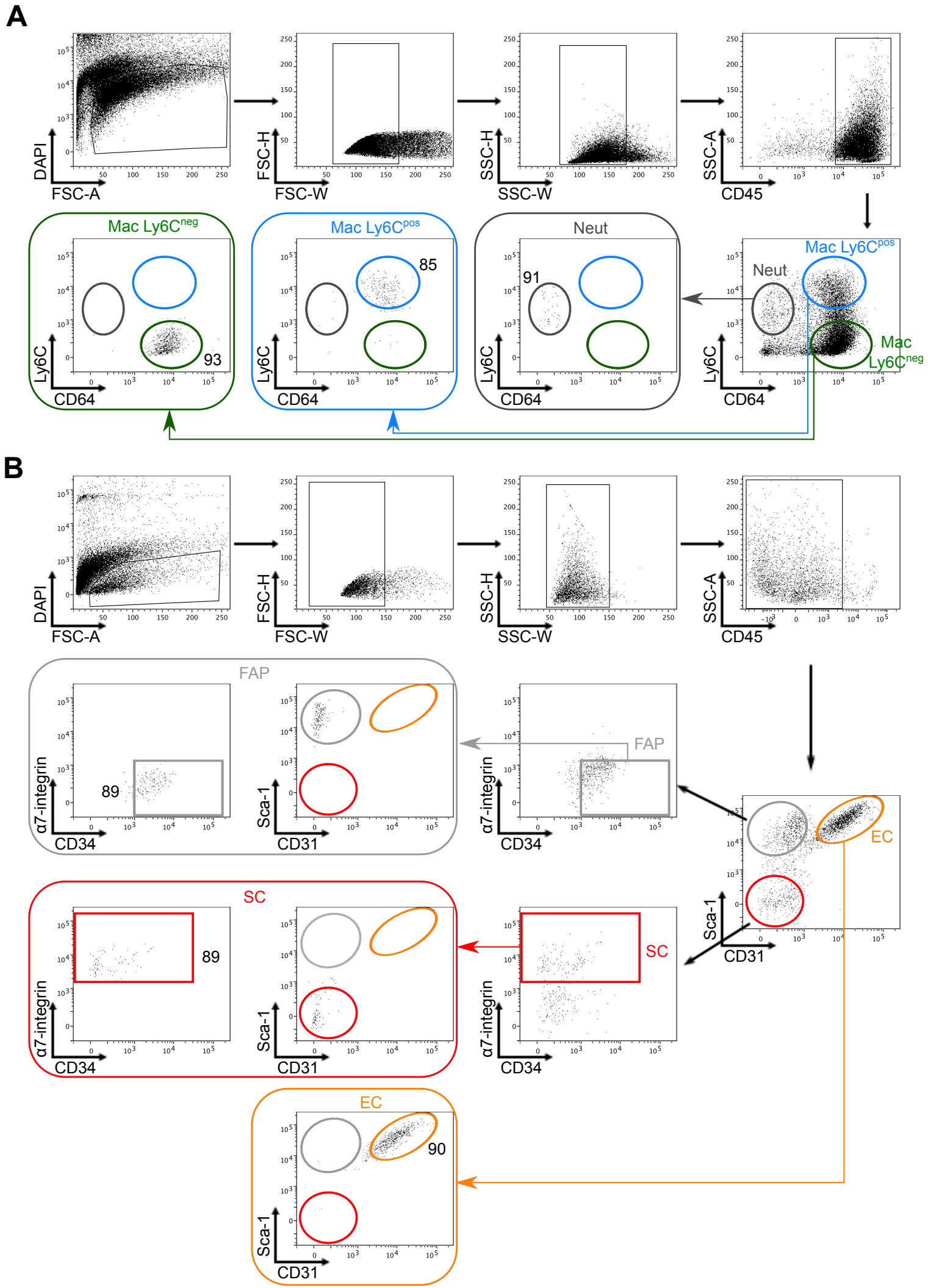

Supplementary Figure 2

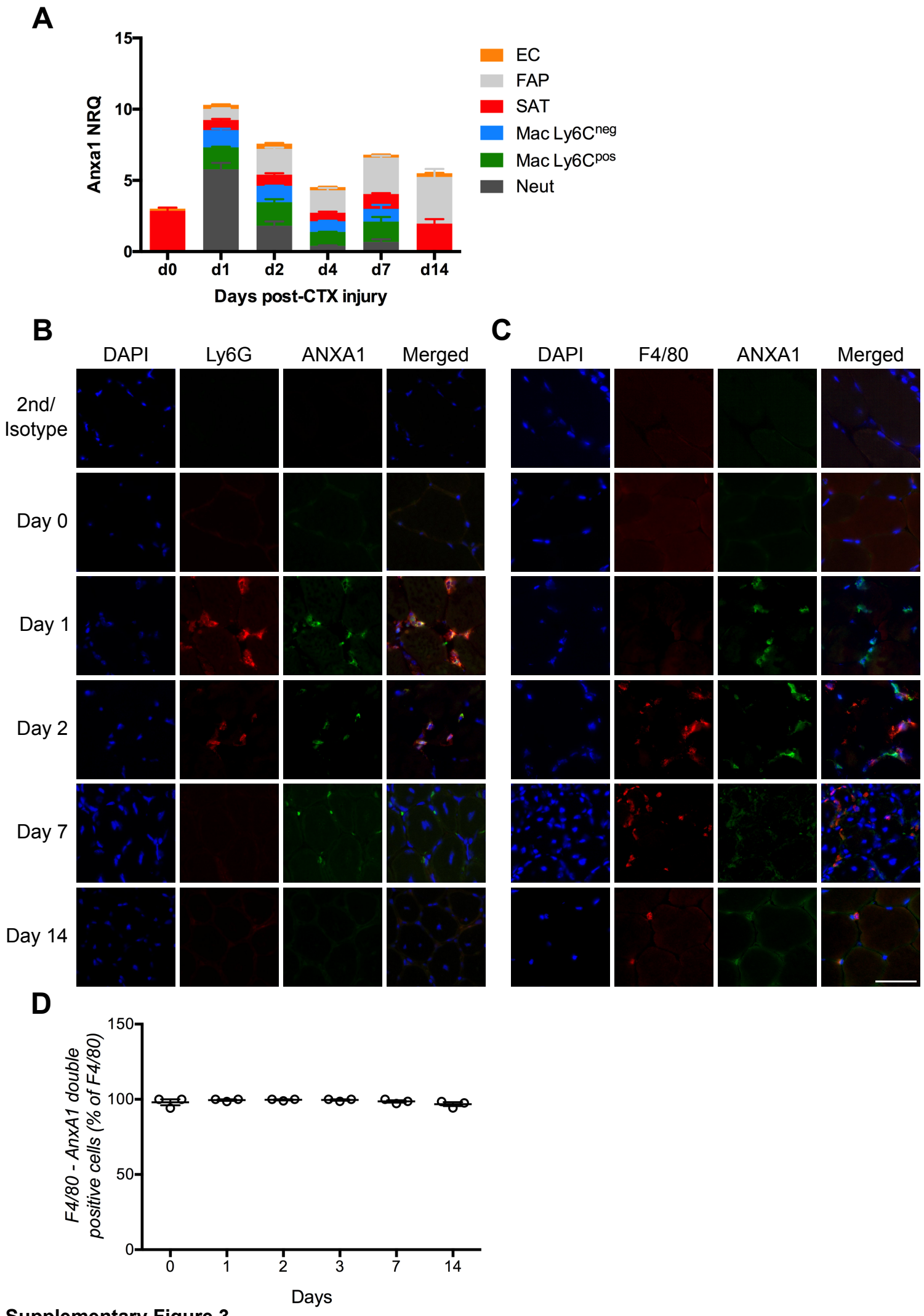

Supplementary Figure 3

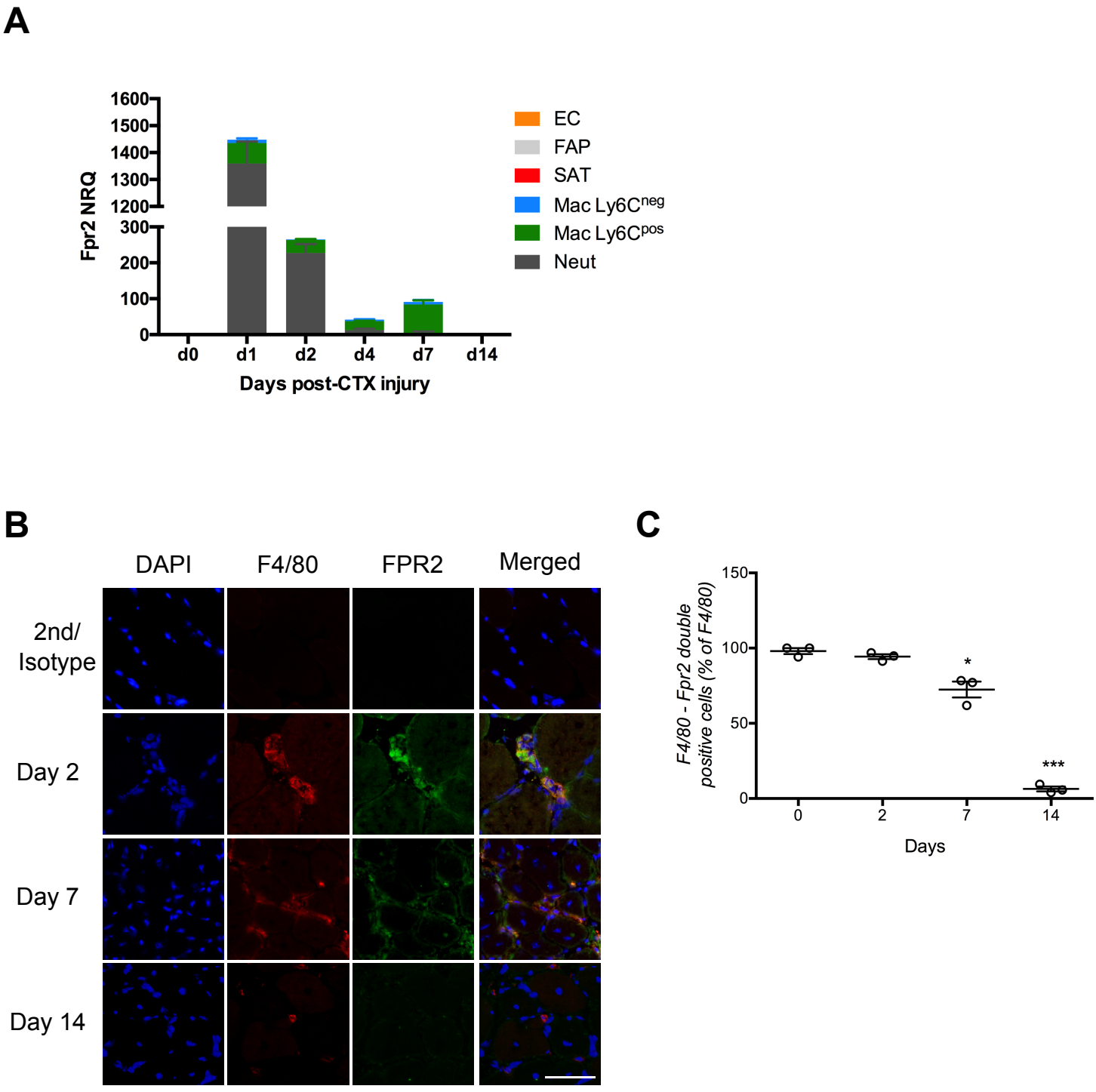

Supplementary Figure 4

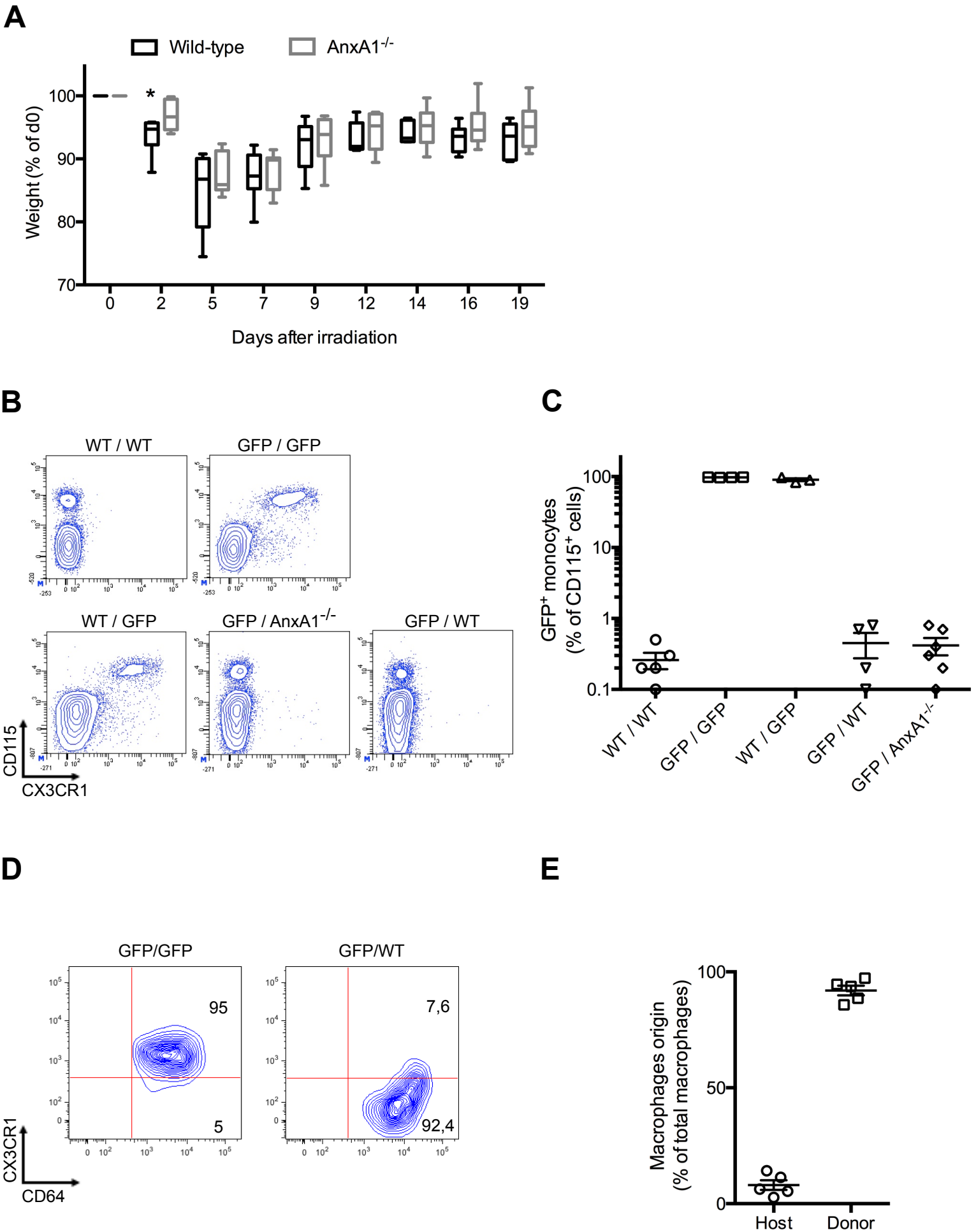

Supplementary Figure 5

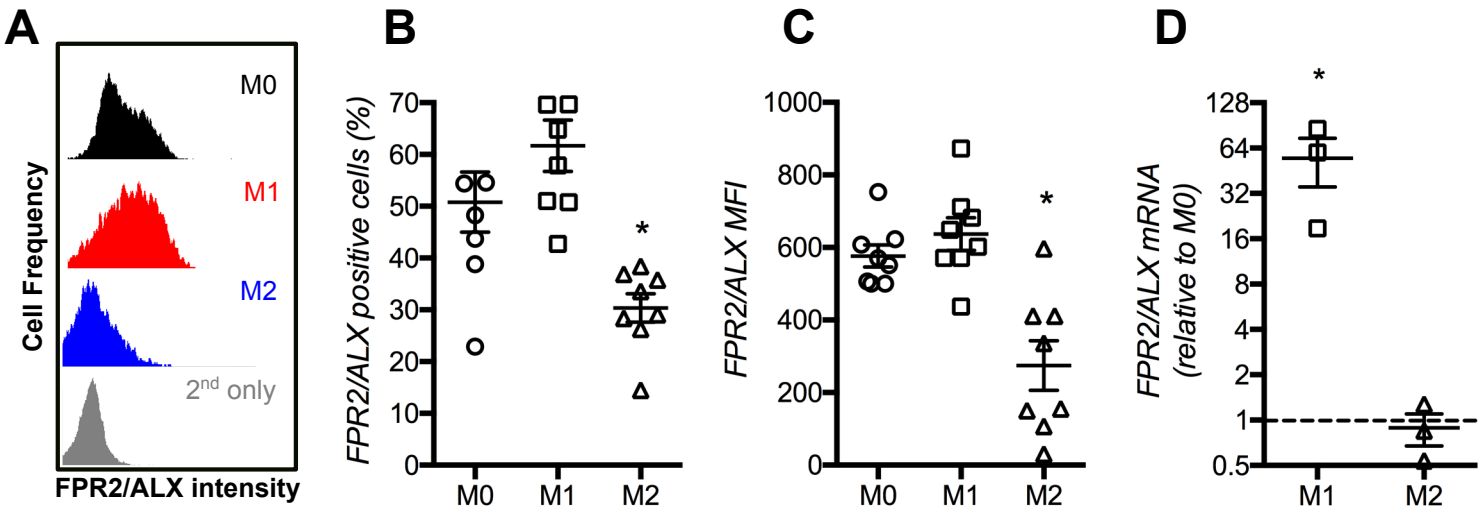

Supplementary Figure 6

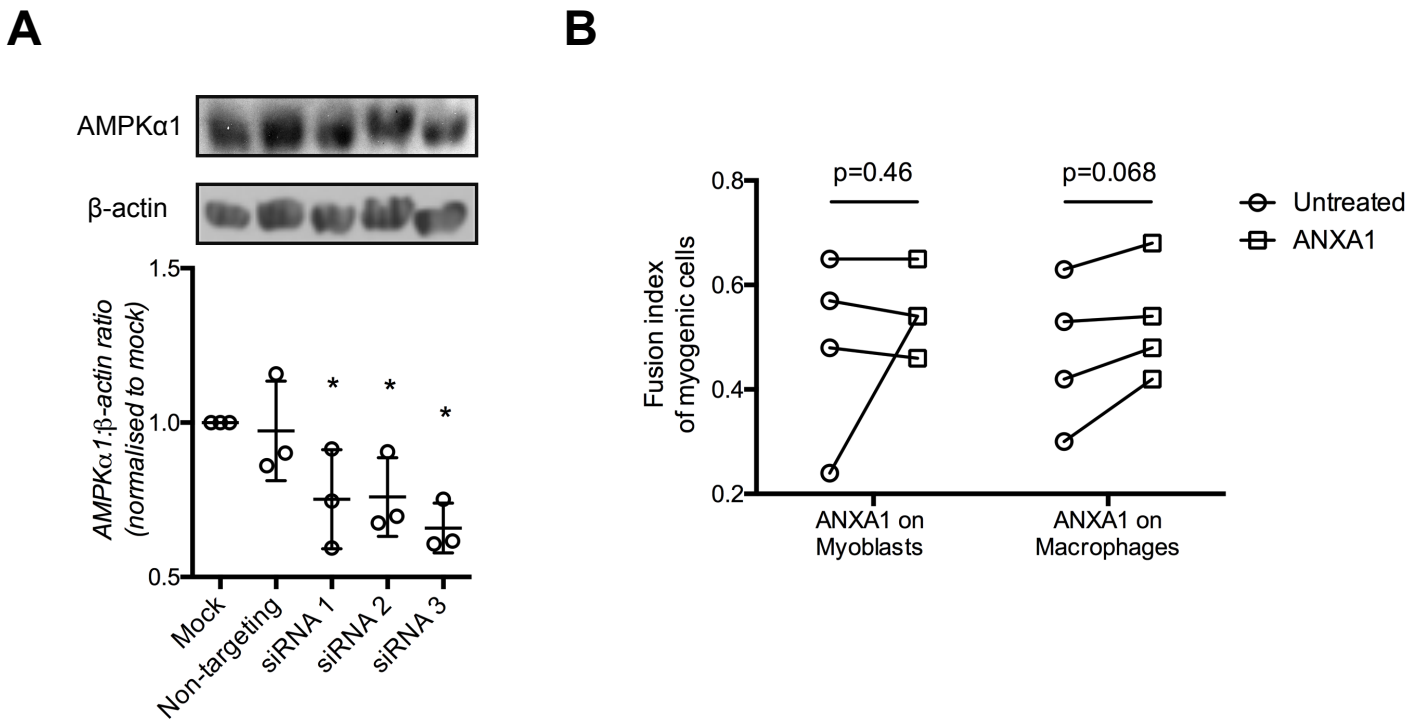

Supplementary Figure 7